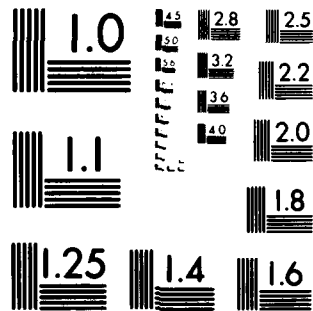


NL

END
DATE
FILMED
6 82
DTIC



MICROCOPY RESOLUTION TEST CHART
NATIONAL BUREAU OF STANDARDS-1963-A

AD A114821

AFOSR-TR- 82 - 0373

JOINT INSTITUTE FOR AERONAUTICS AND ACOUSTICS

NASA

National Aeronautics and
Space Administration

Ames Research Center

JIAA TR-43



Stanford University

**THE STRUCTURE OF A SUBSONIC
COMPRESSIBLE RECTANGULAR JET**

**Y. Hsia, A. Krothapalli, D. Baganoff,
and K. Karamcheti**

STANFORD UNIVERSITY
Department of Aeronautics and Astronautics
Stanford, California 94305-2186

DTIC FILE COPY

JANUARY 1982



Approved for public release;
distribution unlimited.

82 05 24 161
F49620-79-C-0189

UNCLASSIFIED

SECURITY CLASSIFICATION OF THIS PAGE (When Data Entered)

REPORT DOCUMENTATION PAGE		READ INSTRUCTIONS BEFORE COMPLETING FORM
1. REPORT NUMBER AFOSR-TR- 82-0373	2. GOVT ACCESSION NO.	3. RECIPIENT'S CATALOG NUMBER
4. TITLE (and Subtitle) THE STRUCTURE OF A SUBSONIC COMPRESSIBLE RECTANGULAR JET		5. TYPE OF REPORT & PERIOD COVERED INTERIM
		6. PERFORMING ORG. REPORT NUMBER
7. AUTHOR(s) Y HSIA K KARAMCHETI A KROTHAPALLI D BAGANOFF		8. CONTRACT OR GRANT NUMBER(s) F49620-79-C-0189
9. PERFORMING ORGANIZATION NAME AND ADDRESS STANFORD UNIVERSITY DEPT OF AERONAUTICS AND ASTRONAUTICS STANFORD, CA 94305-2186		10. PROGRAM ELEMENT, PROJECT, TASK AREA & WORK UNIT NUMBERS 61102F 2307/A1
11. CONTROLLING OFFICE NAME AND ADDRESS AIR FORCE OFFICE OF SCIENTIFIC RESEARCH/NA BOLLING AFB, DC 20332		12. REPORT DATE JAN 1982
		13. NUMBER OF PAGES 52
14. MONITORING AGENCY NAME & ADDRESS (if different from Controlling Office)		15. SECURITY CLASS. (of this report) UNCLASSIFIED
		15a. DECLASSIFICATION/DOWNGRADING SCHEDULE
16. DISTRIBUTION STATEMENT (of this Report) Approved for public release; distribution unlimited.		
17. DISTRIBUTION STATEMENT (of the abstract entered in Block 20, if different from Report)		
18. SUPPLEMENTARY NOTES		
19. KEY WORDS (Continue on reverse side if necessary and identify by block number) TURBULENT JET HOT WIRE ANEMOMETRY SUBSONIC JET COMPRESSIBLE FLOW RECTANGULAR JET JET STRUCTURE		
20. ABSTRACT (Continue on reverse side if necessary and identify by block number) A subsonic jet of air emanating from a rectangular nozzle of aspect ratio 16.7 has been investigated using hot-wire anemometry. The purpose of this investigation is to extend our knowledge of a rectangular jet from incompressible to compressible flow. Four exit Mach numbers, ranging from 0.18 to 0.8, were selected for the study. Results of the hot-wire measurements show that a compressible subsonic rectangular jet behaves similar to an incompressible jet. It exhibits three distinct regions characterized by the decay of the mean axial velocity along the axis of the jet. These three regions are a potential core region, a		

UNCLASSIFIED

SECURITY CLASSIFICATION OF THIS PAGE(When Data Entered)

two-dimensional type region, and an axisymmetric type region. The effect of increasing the Mach number of the rectangular jet was found to be the extension of the two-dimensional type region, and the jet behaves more nearly like a two-dimensional jet at higher Mach numbers. This effect is due to the variation in the growth rate of the jet in the plane containing the long dimension of the nozzle only. The Mach number has very little effect on the spreading in the plane containing the short dimension of the nozzle. From the distributions of the r.m.s. intensities in the two central planes, it is suggested that the turbulence structure of a compressible rectangular jet can be inferred from that of an incompressible jet.

UNCLASSIFIED

SECURITY CLASSIFICATION OF THIS PAGE(When Data Entered)

JIAA TR - 43

THE STRUCTURE OF A SUBSONIC
COMPRESSIBLE RECTANGULAR JET

Y. Hsia, A. Krothapalli, D. Baganoff, and
K. Karamcheti

DTIC
ELECTE
MAY 25 1982
H

The work here presented has been supported by the
Air Force Office of Scientific Research under
Contract No. F49620-79-0189

AIR FORCE OFFICE OF SCIENTIFIC RESEARCH (AFSC)
NOTICE OF TRANSMISSION TO DTIC
This technical report is being transmitted to DTIC
under the terms of the AFSC-DAAG-19-12.
Distribution is unlimited.
MATTHEW J. KEMPER
Chief, Technical Information Division

ABSTRACT

A subsonic jet of air emanating from a rectangular nozzle of aspect ratio 16.7 has been investigated using hot-wire anemometry. The purpose of this investigation is to extend our knowledge of a rectangular jet from incompressible to compressible flow. Four exit Mach numbers, ranging from 0.18 to 0.8, were selected for the study. Results of the hot-wire measurements show that a compressible subsonic rectangular jet behaves similar to an incompressible jet. It exhibits three distinct regions characterized by the decay of the mean axial velocity along the axis of the jet. These three regions are a potential core region, a two-dimensional type region, and an axisymmetric type region. The effect of increasing the Mach number of the rectangular jet was found to be the extension of the two-dimensional type region, and the jet behaves more nearly like a two-dimensional jet at higher Mach numbers. This effect is due to the variation in the growth rate of the jet in the plane containing the long dimension of the nozzle only. The Mach number has very little effect on the spreading in the plane containing the short dimension of the nozzle. From the distributions of the r.m.s. intensities in the two central planes, it is suggested that the turbulence structure of a compressible rectangular jet can be inferred from that of an incompressible jet.



Accession For	
NTIS GRA&I	<input checked="" type="checkbox"/>
DTIC TAB	<input type="checkbox"/>
Unannounced	<input type="checkbox"/>
Justification	
By	
Distribution/	
Availability Codes	
Dist	Avail and/or Special
A	

ACKNOWLEDGEMENTS

Many in the Joint Institute for Aeronautics and Acoustics contributed suggestions and assisted in various ways in the research, and we would like to thank each for their help.

Special thanks are due to Mr. Vadim Matte whose outstanding work on the facility heating control and hot-wire probes made this experiment possible. The facility and model were expertly made by Messrs Jerry deWerk and Al Armes. Mr. Dale Buermann assisted in the operation of much of the electronics. Our thanks to all of them.

This work was supported by Air Force Office of Scientific Research under contract no. F49620-79-0189.

LIST OF SYMBOLS

D	Nozzle width
E	Mean voltage
E_c	Mean voltage on jet centerline
\bar{E}_{cta}	Constant-temperature anemometer output voltage
E_{cta}	Mean constant-temperature anemometer output voltage
\bar{E}_{lin}	Linearizer output voltage ($= E + e$)
E_{lin}	Mean linearizer output voltage ($= E$)
e	Hot-wire fluctuation voltage
$\langle e \rangle$	Root mean square of e
\hat{e}	Normalized hot-wire fluctuation voltage ($= \langle e \rangle / E_c$)
K	Calibration constant
k	Jet spreading rate
L	Nozzle length
M	Mach number
M_e	Mach number at jet exit
$\langle p' \rangle$	Root mean square of the pressure fluctuation
T	Flow temperature
T_o	Total temperature
T_o'	Total temperature fluctuation
$\langle T_o' \rangle$	Root mean square of T_o'
\bar{U}	Flow velocity ($= U + u$)
U	Mean velocity
U_e	Mean velocity at jet exit

U_o	Mean velocity on jet centerline
u	Velocity fluctuation
$\langle u \rangle$	Root mean square of u
\bar{u}	Turbulence intensity ($=\langle u \rangle / U_o$)
X, Y, Z	Cartesian coordinate system
X_o	Jet virtual origin
X_c	Crossover point coordinate
$Y_{1/2}$	Jet half-velocity width in the central X, Y plane
$Z_{1/2}$	Jet half-velocity width in the central X, Z plane
γ	Specific heat ratio
ρ	Density
$\bar{\rho}$	Mean density
ρ'	Density fluctuation
$\rho \bar{U}$	Mass flow rate
$\overline{\rho U}$	Mean mass flow rate
$(\rho u)'$	Mass flow rate fluctuation
$\langle (\rho u)' \rangle$	Root mean square of $(\rho u)'$

TABLE OF CONTENTS

ABSTRACT	ii
ACKNOWLEDGEMENTS	iii
LIST OF SYMBOLS	iv

<u>Chapter</u>	<u>page</u>
1. INTRODUCTION	1
2. APPARATUS, INSTRUMENTATION, AND PROCEDURES	4
Air Supply System	4
Nozzle Geometry and Coordinate System	6
Flow Visualization System	7
Hot-wire Anemometry and Traversing Mechanism	7
Calibration Equipment and Procedures	9
Interpretation of Hot-wire Signals in Compressible Flow	12
Transonic Effect	13
3. RESULTS AND DISCUSSION	14
Initial Conditions	14
Schlieren Photographs	15
Mean Velocity Field	16
R.m.s. Intensity	19
An Overall View of the Flow Field	20
4. CONCLUSIONS	22
REFERENCES	24

FIGURES

LIST OF FIGURES

1. A Schematic of the Air Supply System
2. Heating Stage of the Air Supply System
 - (a) Strip Heaters Mounted on Two Square Pipes with Switch Board
 - (b) Schematic of the Heating Arrangement and Wiring
3. (a) Schematic of the Rectangular Nozzle Inlet Geometry with a Cartesian Coordinate System
(b) The Multiple-Nozzle Model
4. Schematic of the Flow Visualization (Schlieren) System
5. Signal Processing Instrumentation and Probe Positioning Setup
6. Calibration Curves for the Hot-Wire
7. Measured R.m.s. Intensity \hat{e} and Corrected Turbulence Intensity \hat{u} along the Centerline of the Rectangular Jet at $M_e=0.8$
8. A Rectangular Jet of Exit Mach Number of 0.8
 - (a) Hot-Wire with Its Support in the Flow
 - (b) No Probe in the Flow
9. Mean and R.m.s. Profiles of Hot-Wire Voltage along the Y and Z Axes at the Nozzle Exit for $M_e=0.3, 0.5,$ and 0.8
10. Schlieren Photographs of the Rectangular Jet in the X,Y Plane for Different Exit Mach Numbers(M_e)
 - (a) $M_e=0.3$
 - (b) $M_e=0.5$
 - (c) $M_e=0.8$
11. Schlieren Photographs of the Jet in the X,Z Plane for $M_e=0.8$
12. The Decay of Normalized Centerline Mean Velocity of the Jet for Four Exit Mach Numbers
13. Mean Velocity Profiles in the Central X,Y Plane for Three Exit Mach Numbers
 - (a) $M_e=0.3$
 - (b) $M_e=0.5$
 - (c) $M_e=0.8$
14. Mean Velocity Profiles in the Central X,Z Plane for Three Exit Mach Numbers
 - (a) $M_e=0.3$
 - (b) $M_e=0.5$
 - (c) $M_e=0.8$

15. Growth of a Rectangular Jet with Downstream Distance for Various Exit Mach Numbers
16. Variation of Turbulence Intensity along the Centerline of the Jet for Different Exit Mach Numbers
17. Distribution of Hot-Wire Voltage Fluctuation in the Central X,Y Plane for Three Exit Mach Numbers
 - (a) $M_e=0.3$
 - (b) $M_e=0.5$
 - (c) $M_e=0.8$
18. Distribution of Hot-Wire Voltage Fluctuations in the Central X,Z Plane for Three Exit Mach Numbers
 - (a) $M_e=0.3$
 - (b) $M_e=0.5$
 - (c) $M_e=0.8$
19. Isometric Plots of the Mean and R.m.s. Hot-Wire Voltages for the Jet at $M_e=0.8$

Chapter 1

INTRODUCTION

Rectangular jets have been used in a wide variety of engineering applications such as the augmentor wing ejectors for short-takeoff-and-landing (STOL) aircraft. The present experiment is part of a continuing effort to investigate the mixing of multiple rectangular jets in thrust-augmenting ejectors. Previous work on this subject has been reported by Krothapalli et al.[1]* where emphasis was on the incompressible rectangular jet. The present work concentrates on the structure of a compressible rectangular jet at various subsonic Mach numbers.

The previous investigation has revealed that the flow field of an incompressible rectangular jet can be characterized by the presence of three distinct regions as defined by the decay of the mean axial velocity along the centerline of the jet, U_c . These regions may be classified as follows: a potential core region, where U_c is constant; a two-dimensional type region, where U_c decays close to a self-preserved two-dimensional jet; and an axisymmetric type region, where U_c decays at the same rate as a self-preserved axisymmetric jet. It is known that the extent of each of these regions is a function of the nozzle aspect ratio and inlet geometry. Detailed mean velocity and temperature profiles as well as some turbulence quantities of rectangular jets having different aspect ratios and nozzle geometries were measured using

* Numbers in brackets designate References cited.

hot-wire anemometry by Sfeir [2,3]. Recently, Krothapalli, Baganoff and Karamcheti [4] reported further detailed measurements of an incompressible rectangular jet. While supporting the previous observations [2,3,5-8], these results furnished more turbulence data.

In the cases of thrust augmenting ejectors and jet engines, the jet exit velocities are so high that the flow can no longer be considered as being incompressible. However, none of the fore-mentioned experiments were conducted at velocities high enough to be considered compressible. It is the purpose of this investigation to study the flow structure of a compressible rectangular jet and identify, if any, the effects of Mach number on the jet structure.

In light of past experimental observations [1-8] the characteristics of a rectangular jet are expected to depend upon the following parameters:

- aspect ratio of the nozzle
- inlet geometry of the nozzle
- Mach number at the nozzle exit
- Reynolds number at the nozzle exit
- type of exit velocity profile
- type of boundary layer at the nozzle exit
- magnitude of the turbulence intensity at the exit plane of the nozzle

- condition of the ambient medium into which the jet is issuing

In the present experiment, four exit Mach numbers (0.18, 0.3, 0.5, and 0.8) were chosen. The corresponding Reynolds numbers based on the width of the nozzle extended from 12,000 to 52,000. A nozzle of aspect ratio 16.7 (50 mm long, 3 mm wide) was used in this experiment. The inlet geometry of the nozzle was designed to obtain a low turbulence level at the exit plane.

Chapter 2

APPARATUS, INSTRUMENTATION, AND PROCEDURES

2.1 AIR SUPPLY SYSTEM

A schematic of the air supply system is shown in figure 1. A Worthington Type 280 compressor was used in conjunction with a 104 ft³ storage tank to provide a blow-down type air supply. The compressor is able to raise the pressure in the storage tank at a rate of 150 psi per hour, to a peak pressure of 2800 psi. For the highest mass flow rate used for this investigation (125 kg/hr), a fully charged tank is able to supply the air flow for a period of about two hours.

The high pressure air from the storage tank passes through a shut-off valve and a 0.5 μ m filter before entering a two-stage feedback control regulator. The two-stage regulator is able to drop the pressure to 70 psig or lower and maintain a constant pressure in the settling chamber to an accuracy better than ± 0.1 cmHg, which corresponds to a velocity variation of less than 2 m/sec at the nozzle exit.

Because the air undergoes a throttling process at the regulator, the flow temperature drops considerably. For conditions of this experiment, the maximum temperature drop is about 10°C. Provisions were made to raise the flow total temperature to that of ambient so that the total temperature of the jet remains the same upon mixing with ambient air. This was done by a heating stage which consisted of sixteen strip

heaters (85 cm long and 4 cm wide each) and two square pipes (2 x 2 in² cross section, each 5 ft long). The strip heaters were mounted on the outside walls of the square pipes through which the air passes. A picture of this setup is shown in figure 2a. Only eight of the sixteen heaters were used in this experiment. Each heater, which can produce 7.5 kW of power, was connected to an independent switch. A schematic of the arrangement is shown in figure 2b. The heaters are controlled manually by turning on a certain number of heaters while monitoring the temperature in the settling chamber using a digital thermometer (Doric 410A Digital Trendicator with iron-constantine thermocouple). For the highest flow rate used in this experiment (0.04 kg/sec), the total temperature can be raised up to 40°C above ambient temperature. The temperature in the settling chamber was maintained at a constant temperature, usually at room temperature, to an accuracy of about $\pm 0.5^\circ\text{C}$ over the duration of each test.

After passing through the heating stage, the air is injected into a cylindrical settling chamber through a spray bar (see figure 1) which helps in distributing the flow uniformly. The settling chamber is 1.75 m in length and 0.6 m in diameter. The velocity of the flow in the settling chamber is about 0.14 m/sec for the highest flow rate tested. At the other end of the settling chamber the air is passed through a bell mouth and six fine mesh screens placed 5 cm apart in the exit section of the settling chamber. Following the screen pack, the flow passes through an adapter which connects the model to the settling chamber. The adapter was made to provide a smooth transition from a circular cross section at the exit of the settling chamber to the rectangular

cross section of the model. This experiment made use of the same air supply system as the one used by Krothapalli et al.[1] except for the heating stage. More detailed information on the facility is found in that report.

2.2 NOZZLE GEOMETRY AND COORDINATE SYSTEM

Figure 3a shows the geometry of the rectangular nozzle together with the coordinate system used in this study. The nozzle is 50.0 mm in length (L) and 3.0 mm in width (D), and is preceded by a 40 mm long channel having the same cross section. The nozzle lip has a thickness of 1.5 mm. The convergent entrance region was designed to provide smooth contraction with a contraction ratio of about 36. The nozzle used is the center lobe of a multiple nozzle configuration, as shown in figure 3b, which was designed to study the mixing of multiple rectangular jets [1]. The remaining four lobes were sealed at the inlet section. A 70-degree triangular shaped ventilation entry between the lobes was employed to ensure a smooth induced flow. For the conditions tested, top-hat mean velocity profiles and low turbulence intensities were obtained at the nozzle exit.

A Cartesian coordinate system was used with its origin located at the center of the nozzle and with the X axis oriented along the centerline of the jet. The Y and Z axes are parallel to the short and long dimensions of the nozzle, respectively.

2.3 FLOW VISUALIZATION SYSTEM

A conventional Schlieren system, as shown schematically in figure 4, was adopted for flow visualization. The light source employed is a stroboscopic flash unit (US Scientific Instruments Type 3015 Stroboscope) which can be triggered either manually to produce a single flash or as a stroboscope. The duration of each flash is a function of the light intensity and can be varied from 1.3 to 7.0 μsec at five discrete values. Each of the Schlieren photographs shown in this report was taken using a single flash of 1.5 μsec duration. The collimating and focusing mirrors are spherical mirrors. Their focal lengths (f) and diameters (dia.) are given in the figure. The optics were arranged such that the size of the image was the same as that of the object. Polaroid Type 57 high speed instant film (ASA 3000) was used to obtain the photographs.

2.4 HOT-WIRE ANEMOMETRY AND TRAVERSING MECHANISM

The velocity measurements were made using a linearized constant-temperature hot-wire anemometer. The hot-wire probe was positioned by an orthogonal three-axis traversing mechanism. A schematic of the anemometer with the signal processing instruments and the traversing mechanism is shown in figure 5.

A standard constant-temperature bridge DISA 55M10 in conjunction with a DISA 55P11 single normal wire was used to make the measurements. The wire is a platinum-coated tungsten wire having a 5 μm diameter and a 1 mm length. The frequency response obtained with a square wave test was approximately 40 kHz. All hot-wire measurements were made with the

wire oriented parallel to the Z axis and perpendicular to the X and Y axes. With the objective of the experiment in mind, which was to explore and study the jet behavior at high velocities in terms of global properties rather than detailed information, a single wire was used rather than an X-wire probe.

To linearize the hot-wire signals, a DISA 55M25 Linearizer was used. A linearization range between 20 and 280 m/sec was achieved in this experiment. Details of the calibration procedure are discussed in the next section.

The signals from the linearizer were sent to a TSI (Thermo-Systems Inc.) Type 1076 Digital Voltmeter and a DISA 55D35 R.m.s. Voltmeter for mean and r.m.s. values. The integration time constant can be set in discrete steps from 0.1 to 100 seconds on both voltmeters.

A traversing mechanism supplied by Velmex Corp. was employed to position the hot-wire probe. It has three translational degrees of freedom. Each of the three axes was oriented parallel to an individual coordinate of the Cartesian system chosen (see figure 3a). The vertical axis of the mechanism (parallel to the X axis) was equipped with a Bodine induction synchronous motor which allowed quick positioning of the probe to a required downstream location. The two horizontal axes of the traversing mechanism (parallel to the Y and Z axes) were guided by lead screws and driven separately by two stepper motors. The stepper motor rotates the lead screw through a fixed angle for each pulse sent by the control circuitry. The total angular rotations or the total distance moved can be determined by keeping track of the number of pulses sent to the motor.

The minimum positioning increment is 0.01 mm. The control circuitry can send pulses at a fixed rate as selected by the operator. The circuitry also provides an analog voltage proportional to the relative position of the probe. With this capability, mean and r.m.s. velocity profiles can be recorded in a continuous mode. This was done on two X-Y recorders (HP 7004B and 7046A). The X axes of the recorders were connected to the analog output of the traverse control circuitry while the Y axes were connected separately to the outputs of TSI and DISA voltmeters. Having tested different voltmeter time constants and traversing speeds, it was found that the combination of a 1 second time constant and a traversing speed of approximately 10 mm/min was adequate, and hence used in this experiment.

2.5 CALIBRATION EQUIPMENT AND PROCEDURES

The output voltage of a constant-temperature anemometer (cta) may be expressed in the following form [9]:

$$\tilde{E}_{cta}^2 = A + B (\rho \tilde{U})^n \quad (1)$$

where \tilde{E}_{cta} is the anemometer output voltage, ρ and \tilde{U} are the density and velocity of the fluid, respectively, at the point where the hot-wire sensor is located, and A, B and n are constants to be determined experimentally. The value of the exponent n is always close to 0.5. Equation (1) shows that the anemometer output voltage is a nonlinear function of the mass flow rate $\rho \tilde{U}$. The DISA 55M25 Linearizer accomplishes the linearization by means of an analog computer having a transfer function of the following form:

$$\tilde{E}_{lin} = K_1 (\tilde{E}_{cta}^2 - A)^m \quad (2)$$

where \tilde{E}_{lin} , K_1 and m are the linearizer output voltage, a constant and the exponent, respectively. In the particular case of the DISA 55M25 Linearizer the exponent m can be made velocity dependent, $m=m(\tilde{U})$. Substitution of Eq.(1) in (2) gives

$$\tilde{E}_{lin} = K_1 B^m (\rho \tilde{U})^{mn} \quad (3)$$

In the case of incompressible flows, the density is constant and letting $m=1/n$ a direct proportionality between \tilde{E}_{lin} and \tilde{U} is given

$$\tilde{E}_{lin} = K \tilde{U} \quad (4)$$

where K is chosen by the linearizer gain control.

In compressible flow the density ρ can be expressed as a function of the velocity \tilde{U} and then with a properly chosen $m(\tilde{U})$ a direct relationship between the linearizer voltage and the flow velocity can also be achieved. A cold jet exhausting into a medium at rest is an example of such a flow and has been used to calibrate the hot-wire. This flow was supplied by a DISA 55090 Calibration Equipment. The equipment requires a compressed air supply of 200 psig to produce a free air jet, at low turbulence level, for a velocity range between 0.5 and 310 m/sec. The jet velocity with correction for compressibility is available as an analog voltage that can be used to plot the calibration curve on an X-Y recorder.

Although this equipment permits rapid and efficient calibration, it has no control of the flow temperature which is dependent upon the air supplied. Knowing the difference between the calibration temperature and that of the flow being measured, one could use analytical formulas to make corrections on the hot-wire measurements. However, the present experiment used a different approach to eliminate the error. The procedure is described as follows.

After linearization is achieved on the DISA calibrator, the hot-wire is placed at the center of the exit of the rectangular nozzle. Since the flow at the nozzle exit is isentropic and uniform, the velocity can be calculated from the total pressure and temperature by the isentropic flow relations. Keeping the total temperature the same as that of the ambient air and varying the total pressure, the linearizer gain is adjusted such that the calibration constant K equals the selected value. This procedure was repeated before each test run and the temperature was kept the same during the test. Figure 6 shows the resulting linearized relation between the mean hot-wire output voltage and the mean flow velocity for the range between 20 and 280 m/sec with the calibration constant K equal to $1/28$. The deviation of the output voltage from a straight line is less than $\pm 1\%$ for velocities higher than 40 m/sec. The cta bridge voltage is also included in the figure to show the nonlinear relation between the mean cta voltage E_{cta} and the mean velocity U . Using the same procedure, different velocity ranges were chosen for measurements in jets at different exit Mach numbers. For each calibration range, the maximum output voltage of the linearizer was adjusted to be equal to 10.0 volts (maximum linearizer output) for the best resolution.

2.6 INTERPRETATION OF HOT-WIRE SIGNALS IN COMPRESSIBLE FLOW

For measurements in a "steady" turbulent jet, the linearizer output voltage \tilde{E}_{lin} can be decomposed into a time-averaged mean voltage E and a fluctuation voltage e ,

$$\tilde{E}_{lin} = E + e$$

where the time average of e is zero by definition. E is directly proportional to the mean velocity U as the calibration shown in figure 6. The fluctuation voltage e , however, is dependent upon fluctuations in mass flow rate, $(\rho u)'$, and in total temperature, T_o' . Since the total temperatures between the jet flow and ambient are equal in the present study, it may be assumed that the total temperature fluctuation T_o' is negligible and e becomes a measure of $(\rho u)'$ only.

To separate u from $(\rho u)'$, Horstman and Rose [10] suggested an analytical formula with an assumption that $\langle p' \rangle$ (r.m.s. of the pressure fluctuation) is negligible. By letting $\langle T_o' \rangle$ and $\langle p' \rangle$ be zero, the formula given by Horstman and Rose [10] can be simplified to

$$\frac{\langle u \rangle}{U} = \frac{1}{1 + (\gamma - 1)M} \cdot \frac{\langle (\rho u)' \rangle}{\rho U} \quad (5)$$

where M is the Mach number of the flow at the sensor location and γ the specific heat ratio. By assuming the flow to be locally isentropic, the Mach number M can be calculated from mean velocity U . Using the value of $\langle e \rangle / E$ for $\langle (\rho u)' \rangle / \rho U$ in equation (5), $\langle u \rangle / U$ can be found. This

method was used to find $\langle u \rangle / U$ (denoted as \hat{u}) from measured $\langle e \rangle / E (= \hat{e})$ along the centerline of the jet for exit Mach number of 0.8. A comparison of the values between \hat{u} and \hat{e} is displayed in figure 7. At $X/D=150$, the flow velocity is about 50 m/sec which is essentially an incompressible flow but the formula still gives about 5 per cent correction for \hat{u} . Because of this doubtful result, no attempt is made here to incorporate any compressibility corrections to the velocity fluctuations. The fluctuation quantities will be expressed as r.m.s. of fluctuation voltage, $\langle e \rangle$, normalized with centerline mean voltage E_c at the station in question and expressed as \hat{e} which, in an incompressible flow, is equivalent to \hat{u} .

2.7 TRANSONIC EFFECT

According to Liepmann and Roshko [11], a flow is called transonic if both subsonic and supersonic regions are present in the flow field. By this definition a jet of exit Mach number of 0.8 is a bona fide subsonic flow. However, as soon as a probe is inserted in the flow, it may become transonic and the flow characteristics may be changed.

To ensure that such an effect is not found in this experiment, the hot-wire with its support was placed in the potential core of the rectangular jet at the highest exit Mach number tested (0.8) and investigated using Schlieren system. Figures 8a and b show the flow with and without the probe in place. On comparing these two photographs, no obvious effect of the probe is noticed.

Chapter 3

RESULTS AND DISCUSSION

In this chapter, most of the measurements presented are for exit Mach numbers (M_e) of 0.3, 0.5 and 0.8. For comparison purposes, wherever appropriate, results of the incompressible jet exiting at M_e equal to 0.18, taken from a previous investigation [4], are included.

3.1 INITIAL CONDITIONS

It is known that the development of a rectangular jet depends on the conditions at the nozzle exit. In the present investigation, the conditions at the nozzle exit have been studied using the hot-wire and presented in figure 9. The mean and r.m.s. hot-wire voltages along the Y and Z axes at the nozzle exit are recorded for M_e equal to 0.3, 0.5 and 0.8. The profiles along the Y axis have been stretched ten times as wide as those along the Z axis in order to show the details in the short dimension of the jet. For optimum resolution of the profile, different calibration constants K (defined as $E=KU$) were chosen (by varying the linearizer gain) to make the measurements in the jet for different Mach numbers.

Along the Y axis, top-hat mean voltage profiles were obtained for all three exit Mach numbers. The r.m.s. profiles along the Y axis show peaks in the shear layers on either side of the jet. The r.m.s. intensity ($\langle e \rangle / E_c$) in the shear layer increases with Mach number. At the

center of the nozzle exit, the r.m.s. intensities are 0.3%, 0.3% and 0.45% for M_e equal to 0.3, 0.5 and 0.8, respectively.

Along the Z axis, top-hat mean voltage profiles were also obtained except for slight variations close to the jet boundaries (approximately 10 mm inside the boundary). The r.m.s. profiles show spikes at the jet boundaries and the r.m.s. intensity ($\langle e \rangle / E_c$) of the peak increases with M_e . At the Z coordinate corresponding to the location where the mean voltage profile shows non-uniformity, the r.m.s. profile has a local maximum value which decreases in magnitude as M_e increases. It is suggested that this local turbulence may be a result of the secondary flow generated in a rectangular channel ahead of the nozzle exit (see Schlichting [12]).

3.2 SCHLIEREN PHOTOGRAPHS

To study the jet qualitatively, Schlieren photographs of the jet with various exit Mach numbers were taken. Figures 10a,b,c show pictures of the jet in the plane containing the short dimension (X,Y plane) of the nozzle for M_e equal to 0.3, 0.5 and 0.8. These pictures show the flow field of the jet from the nozzle exit to a downstream distance of about 30 nozzle widths. No significant variation in the spreading rate of the jet with Mach number is noticed in these photographs.

Figure 11 shows the jet for M_e equal to 0.8 in the plane containing the long dimension (X,Z plane) of the nozzle. Within the field of observation, very little spreading of the jet is observed, indicating that the flow is nearly two-dimensional. Photographs of the jet for M_e

equal to 0.3 and 0.5 are not included because of their poor contrast; they show similar features as that for M_e equal to 0.8.

3.3 MEAN VELOCITY FIELD

The variation of the (squared) normalized mean velocity along the centerline of the jet for four exit Mach numbers is shown in figure 12. The centerline mean velocity is normalized with respect to the mean velocity at the center of the nozzle exit. The three regions of an incompressible rectangular jet as described in Chapter 1 can be identified in this figure. The first region is the potential core where the centerline mean velocity U_c is constant. It extends from the nozzle exit to a downstream location of about 5D. In the second region, so called two-dimensional type region, the decay rate is close to that of a two-dimensional jet, $(U_c/U_0)^2 \propto X^{-1}$. In the third region, the jet centerline mean velocity decays similar to an axisymmetric jet, $(U_c/U_0)^2 \propto X^{-2}$, hence called axisymmetric type region. It is observed that the transition from the second to the third region seems to occur slightly farther downstream as M_e increases. It appears that the jet decay rate has a fairly weak dependence on the Mach number.

Figures 13a,b,c show the distribution of mean velocity (U) in the central X,Y plane at different downstream locations, ranging from 20 to 100 nozzle widths(D) for various exit Mach numbers. The velocity U is normalized with respect to U_c at the corresponding downstream location while the distance Y is normalized by the distance X to the station in question. The similarity profile for a plane turbulent jet, from Heskestad [13], is shown for comparison in each of the plots. Within

the limits of error for the experiment, at each Mach number the profiles are geometrically similar. The shape of the similarity profile is nearly independent of the exit Mach number and similar to that of a two-dimensional jet. The similarity profile for an incompressible rectangular jet [4] is included in figure 13c. It appears that in the central X,Y plane, compressibility does not introduce a significant effect on the self-similarity of the mean velocity profile.

Figures 14a,b,c show normalized mean velocity profiles in the central X,Z plane at five downstream locations for various exit Mach numbers. At each corresponding downstream location, the profile shows only slight variation with M_e . At $X=20D$, a saddle shape profile is observed in the jet of M_e equal to 0.3. This type of profile was also observed in the two-dimensional type region of incompressible rectangular jets [1-7]. As the exit Mach number increases to 0.5 and 0.8, the saddle shape becomes less pronounced. These mean velocity profiles suggest that in the two-dimensional type region the jet behaves more nearly like a two-dimensional jet at higher subsonic Mach numbers. The similarity profile in the central X,Y plane (figure 13) is also included in figure 14. On comparing the profiles between the two central planes, it is observed that the location where the profiles in both planes are identical seems to move slightly downstream with increasing Mach number. As will be seen later, this location corresponds to the "crossover point". Downstream from this point, the shape of the profile approaches that of an axisymmetric jet as observed in the incompressible jet [4]. The profile of a self-preserved axisymmetric jet measured by Wygnanski and Fiedler [14] is included in figure 14a. As compared to an incompressible jet,

the variations noted above are not significant enough to have a major influence on the overall development of the jet.

The growth of the jet with downstream distance in the central X,Y and X,Z planes can be represented by the half-velocity widths $Y_{1/2}$ and $Z_{1/2}$, respectively, as shown in figure 15 for different exit Mach numbers. The half-velocity width is defined as the distance from the centerline of the jet to the point where the axial mean velocity is equal to one-half of its centerline value. The jet in the X,Y plane spreads linearly with X and the locus of the half-velocity points is given by

$$Y_{1/2} = k (X - X_0)$$

where k is the spreading rate and X_0 the virtual origin. The values of k and X_0 are unchanged for M_e varying from 0.3 to 0.8 ($k=0.11$, $X_0=-2.00$) and show very little difference from those of an incompressible jet at M_e equal to 0.18 ($k=0.109$, $X_0=-2.50$) [4]. The exit Mach number seems to have very little effect on the growth of the jet in the X,Y plane.

However, in the central X,Z plane the variation of the half-velocity width with X shows some changes with exit Mach number. For M_e equal to 0.3, 0.5 and 0.8, $Z_{1/2}$ varies only slightly with X. But in the incompressible jet ($M_e=0.18$) [4], $Z_{1/2}$ first decreases with downstream location X and then increases. At some intermediate location the half-velocity widths in the two central planes cross over. This location corresponds to the onset of the axisymmetric type region. The distance from the nozzle exit to the crossover point along the X axis is denoted

as X_c . It is noted that X_c increases with increasing Mach number, which is solely due to the variation of $Z_{1/2}$ with the exit Mach number.

3.4 R.M.S. INTENSITY

The r.m.s. values of hot-wire voltage fluctuations on the centerline of the jet normalized with the local mean, $\hat{e} (=e/E_c)$, for four different exit Mach numbers are shown in figure 16. The variations of \hat{e} along the jet centerline for all four Mach numbers follow the same pattern. The magnitude of \hat{e} increases sharply in the potential core region. In the two dimensional type region, \hat{e} either decreases or maintains a constant value with X and then increases gradually. The gradual increase in \hat{e} is continued in the axisymmetric type region. For X greater than about 600, the magnitude of \hat{e} at a given downstream location seems to decrease with increasing M_e .

The behavior of \hat{e} described above for X less than 300 is very similar to that of a rectangular jet with laminar boundary layers at the nozzle exit as reported by Hill, Jenkins and Gilbert [15] (aspect ratio 10.5). They also found that, when the boundary layers are turbulent, \hat{e} increases monotonically with X . On comparing the variations of \hat{e} in figure 16 with the results in Ref.15, it may be concluded that the boundary layers in the present experiment are laminar for all four exit Mach numbers tested. However, the turbulence intensity in the boundary layer at the nozzle exit for M_e equal to 0.8 was found to be about 10% (see figure 9), which led us to believe that the boundary layer might be turbulent. Due to the small size of the nozzle, no measurements could be made in the boundary layer to justify either one of the above statements.

Profiles of \hat{e} in the central X,Y plane at different downstream locations are shown in figures 17a,b,c, for various exit Mach numbers. A distinct saddle shape is observed in the profiles in both two-dimensional and axisymmetric type regions. The \hat{e} profiles indicate geometrical similarity only in the two-dimensional type region of the jet ($200 < X < 800$). This was also observed in the incompressible jet [4]. For X greater than 800 (i.e. in the so-called axisymmetric type region), the magnitude of \hat{e} near the jet centerline increases and the profiles approach that of an axisymmetric jet (see figure 4 of [14]). This behavior is believed to be a result of the merging of the two shear layers separated by the long dimension of the nozzle.

Profiles of \hat{e} in the central X,Z plane are shown in figures 18a,b,c for different M_e . On comparing these profiles with the corresponding mean velocity profiles in figure 14, the point of maximum turbulence intensity coincides with the point where the velocity gradient ($\partial U / \partial Z$) is maximum. The development of the profiles with downstream distance in the present case is quite similar to those found in an incompressible jet [4].

3.5 AN OVERALL VIEW OF THE FLOW FIELD

In order to provide an overall picture of the development of a rectangular jet, isometric plots were made from mean and r.m.s. hot-wire voltages of the jet with M_e equal to 0.8 at three downstream locations (150, 400 and 900), as shown in figure 19. Due to the symmetry of the jet about the central X,Y plane, only one half of the profiles are displayed. At X equal to 150, the jet is nearly two dimensional with a

typical saddle shape r.m.s. profile in the X,Y plane. Moving downstream to 40D, the jet spreads in the X,Y plane but with no apparant growth in the X,Z plane. At X equal to 90D, both mean and r.m.s. profiles become almost axisymmetric about the X axis with a weak saddle shape r.m.s. profile; and the jet flow seems to have lost its memory of the nozzle geometry.

Chapter 4

CONCLUSIONS

Based on the results discussed in Chapter 3 the following conclusions are drawn. In the case of a subsonic rectangular jet, the general characteristics of the flow field do not change significantly with exit Mach number. Similar to the case of an incompressible rectangular jet, the mean flow field of the jet is characterized by the presence of three distinct regions as defined by the decay of the centerline mean velocity. These three regions are: a potential core region, a two-dimensional type region, and an axisymmetric type region. The onset of the second region where the shear layers separated by the short dimension of the nozzle meet appears to be independent of the jet exit Mach number. However, the location where the shear layers separated by the long dimension of the nozzle meet seems to occur farther downstream with increasing Mach number.

From the measurements in the central X,Y plane of the jet, the following conclusions can be drawn. The mean velocity profiles are geometrically similar with the shape of the profile almost identical to that of an incompressible two-dimensional jet. The half-velocity width of the jet varies linearly with downstream distance, with its slope and virtual origin nearly independent of the exit Mach number. The r.m.s. profiles show self-similarity only in the two-dimensional type region with their shape being independent of the Mach number. In the

axisymmetric type region, no geometrical similarity was observed in those profiles.

In the central X,Z plane, the saddle shape mean velocity profile observed in the two-dimensional type region of an incompressible jet becomes less pronounced as the exit Mach number increases. This observation along with the results in the X,Y plane suggests that the jet behaves more nearly like a two-dimensional jet at higher Mach numbers for downstream locations less than 100D.

From these results, it appears that for a given nozzle geometry the overall properties of a subsonic compressible rectangular jet are quite similar to that of an incompressible jet. It may be suggested that the turbulence structure of a compressible rectangular jet can be inferred from the measurements of an incompressible rectangular jet.

REFERENCES

1. Krothapalli, A., Baganoff, D. and Karamcheti, K., "An Experimental Study of Multiple Jet Mixing", JIAA TR-43, Stanford University, June 1979.
2. Sfeir, A.A., "The Velocity and Temperature Fields of Rectangular Jets", International Journal of Heat and Mass Transfer, Vol. 19, 1976, pp. 1289-1297.
3. Sfeir, A.A., "Investigation of Three-Dimensional Turbulent Rectangular Jets", AIAA Journal, Vol. 17, No. 10, Oct. 1979, pp. 1055-1060.
4. Krothapalli, A., Baganoff, D. and Karamcheti, K., "On the Mixing of a Rectangular Jet", Journal of Fluid Mechanics, Vol. 107, June 1981, pp. 201-220.
5. Sforza, P.M., Steiger, M.H. and Trentacoste, N., "Studies on Three-Dimensional Viscous Jets", AIAA Journal, Vol. 4, No. 5, May 1966, pp. 800-806.
6. Trentacoste, N. and Sforza, P., "Further Experimental Results for Three-Dimensional Free Jets", AIAA Journal, Vol. 5, No. 5, May 1967, pp. 885-891.
7. Trentacoste, N. and Sforza, P.M., "Some Remarks on Three-Dimensional Wakes and Jets", AIAA Journal, Vol. 6, No. 12, Dec 1968, pp. 2454-2456.
8. Yevdjevich, V.M., "Diffusion of Slot Jets with Finite Orifice Length-Width Ratios", Hydraulics Papers, Colorado State University, Fort Collins, Colorado, March 1966.
9. Norman, B., "Hot-Wire Anemometer Calibration at High Subsonic Speeds", DISA Information, No. 5, June 1967.
10. Horstman, C.C. and Rose, W.C., "Hot-wire Anemometry in Transonic Flow", AIAA Journal, Vol. 15, No. 3, March 1977, pp. 395-401.
11. Liepmann, H.W. and Roshko, A., Elements of Gasdynamics, New York, John Wiley & Sons, Inc., 1957, pp. 270-283.
12. Schlichting, H., Boundary-Layer Theory, New York, McGraw-Hill Book Co., 6th ed., 1968, pp. 575-578.
13. Heskestad, G., "Hot-wire Measurements in a Plane Turbulent Jet", Journal of Applied Mechanics, 85E, Dec. 1965, pp. 721-734.

14. Wagnanski, I. and Fiedler, H., "Some Measurements in the Self-Preserving Jet", Journal of Fluid Mechanics, Vol.38, Part 3, 1968, pp.577-612.
15. Hill Jr., W.G., Jenkins, R.C. and Gilbert, B.L., "Effects of the Initial Boundary-Layer State on Turbulent Jet Mixing", AIAA Journal, Vol.14, No.11, Nov. 1976.

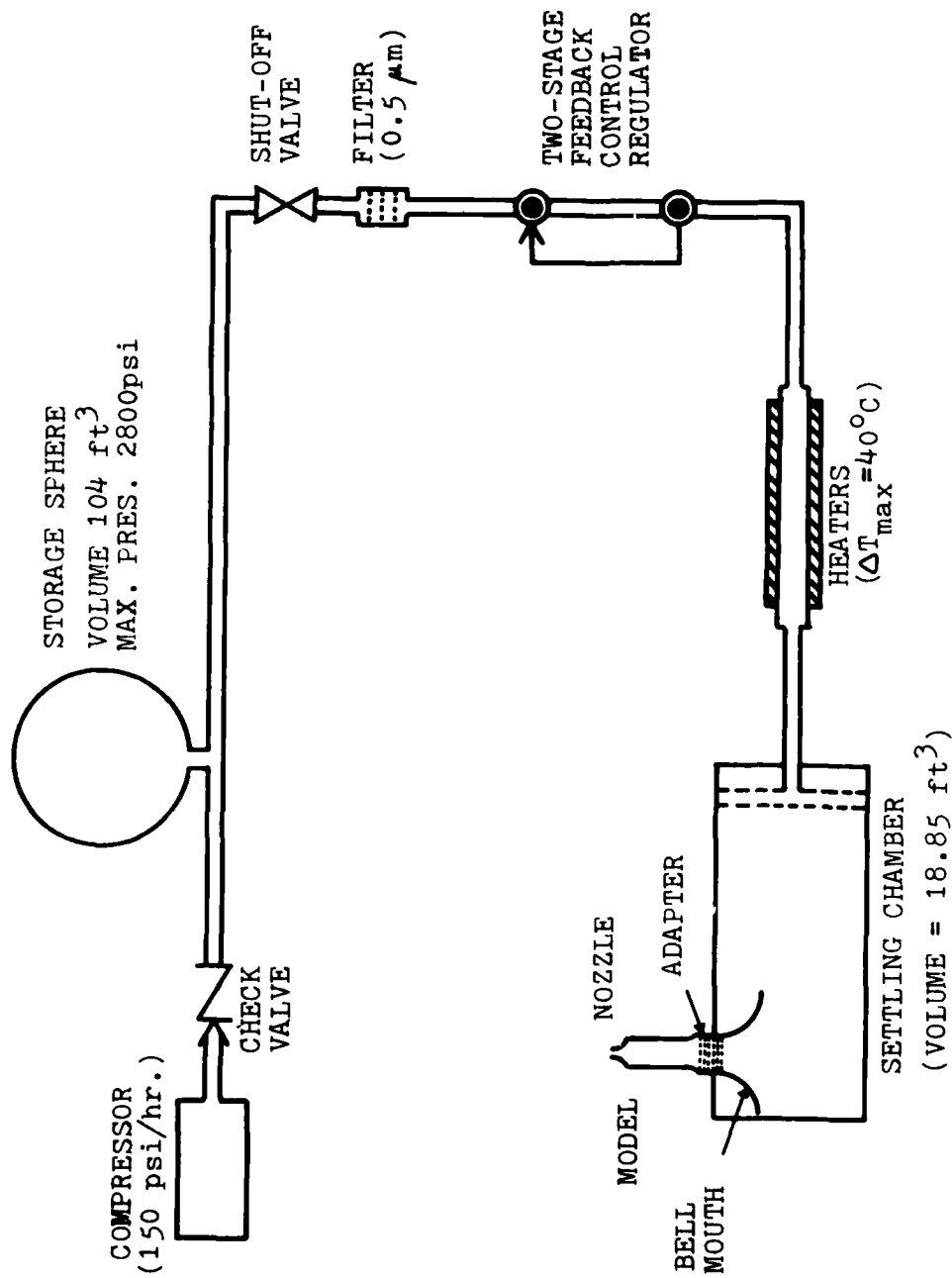
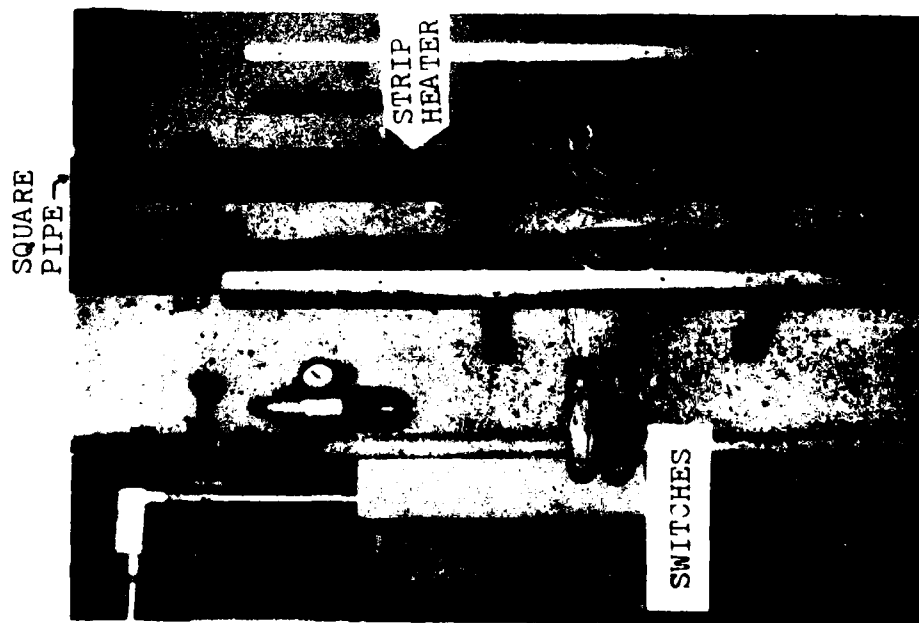
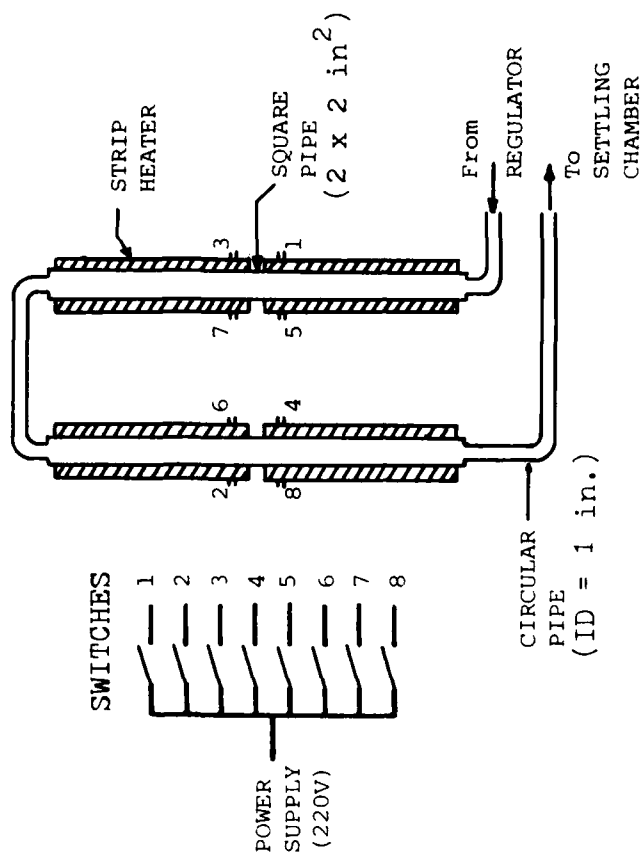


Figure 1 A schematic of the air supply system

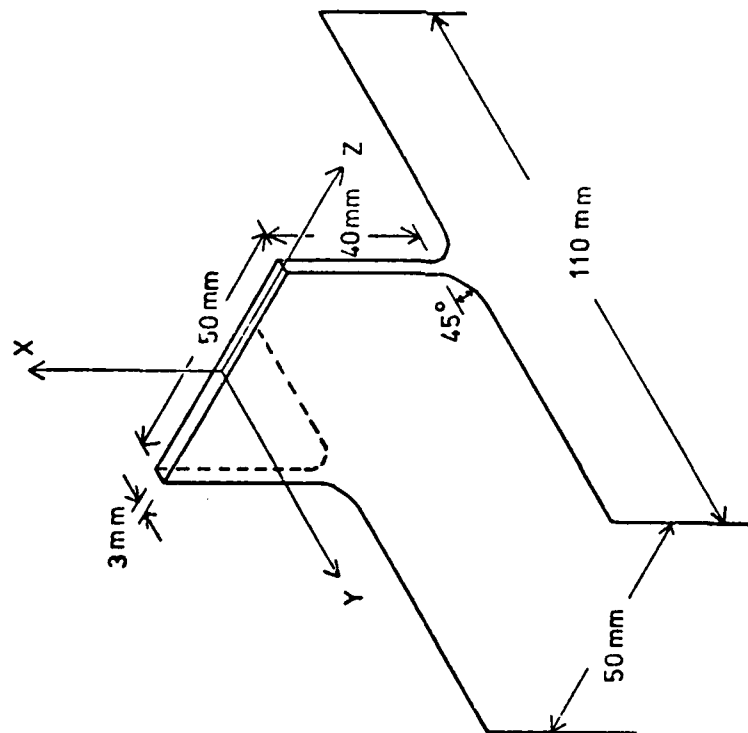


(a)

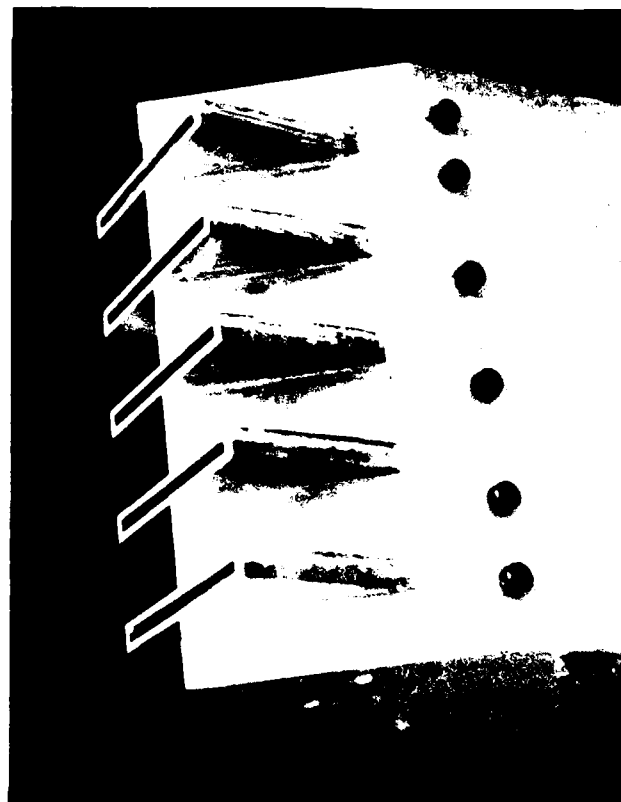


(b)

Figure 2 Heating stage of the air supply system
 (a) Strip heaters mounted on two square pipes with switch board
 (b) Schematic of the heating arrangement and wiring



(a)



(b)

Figure 3 (a) Schematic of the rectangular nozzle inlet geometry with a Cartesian coordinate system
(b) The multiple-nozzle model

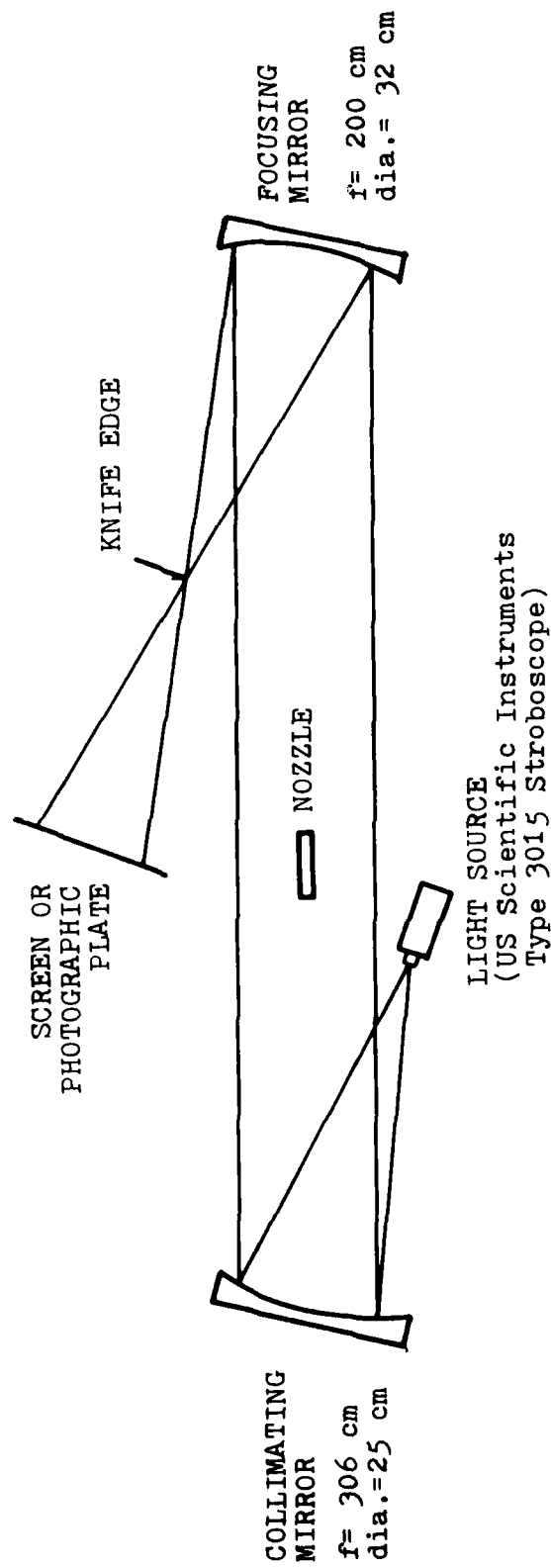


Figure 4 Schematic of the flow visualization (Schlieren) system

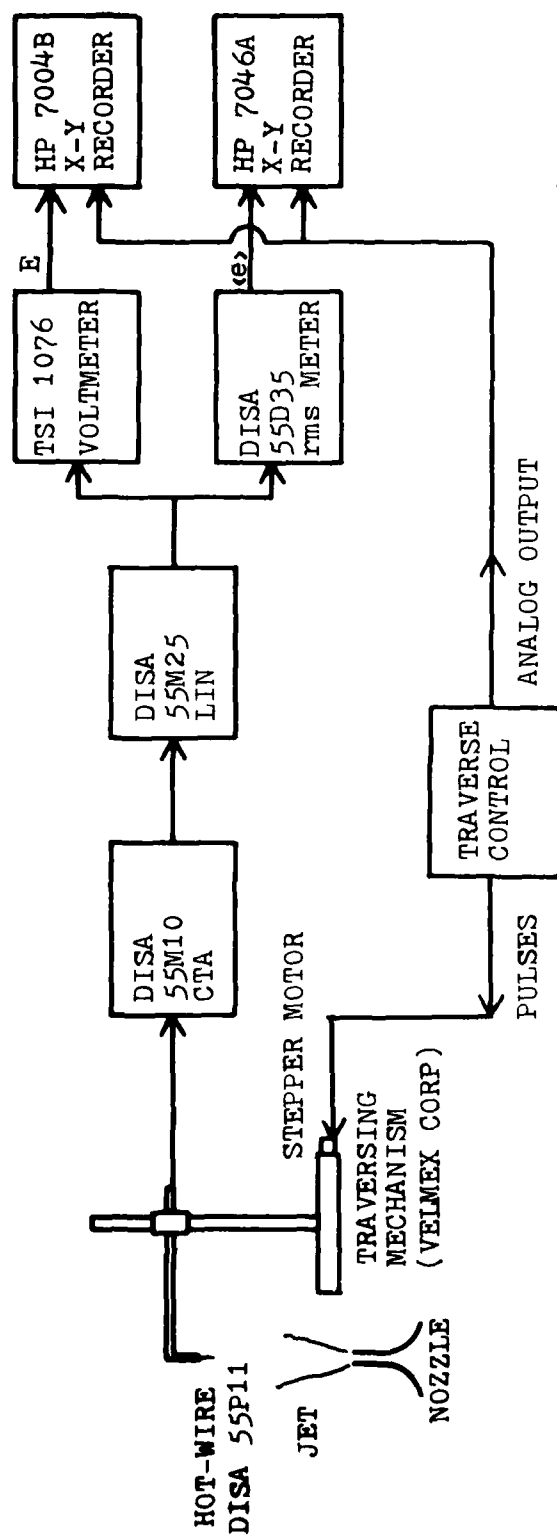


Figure 5 Signal processing instrumentation and probe positioning setup

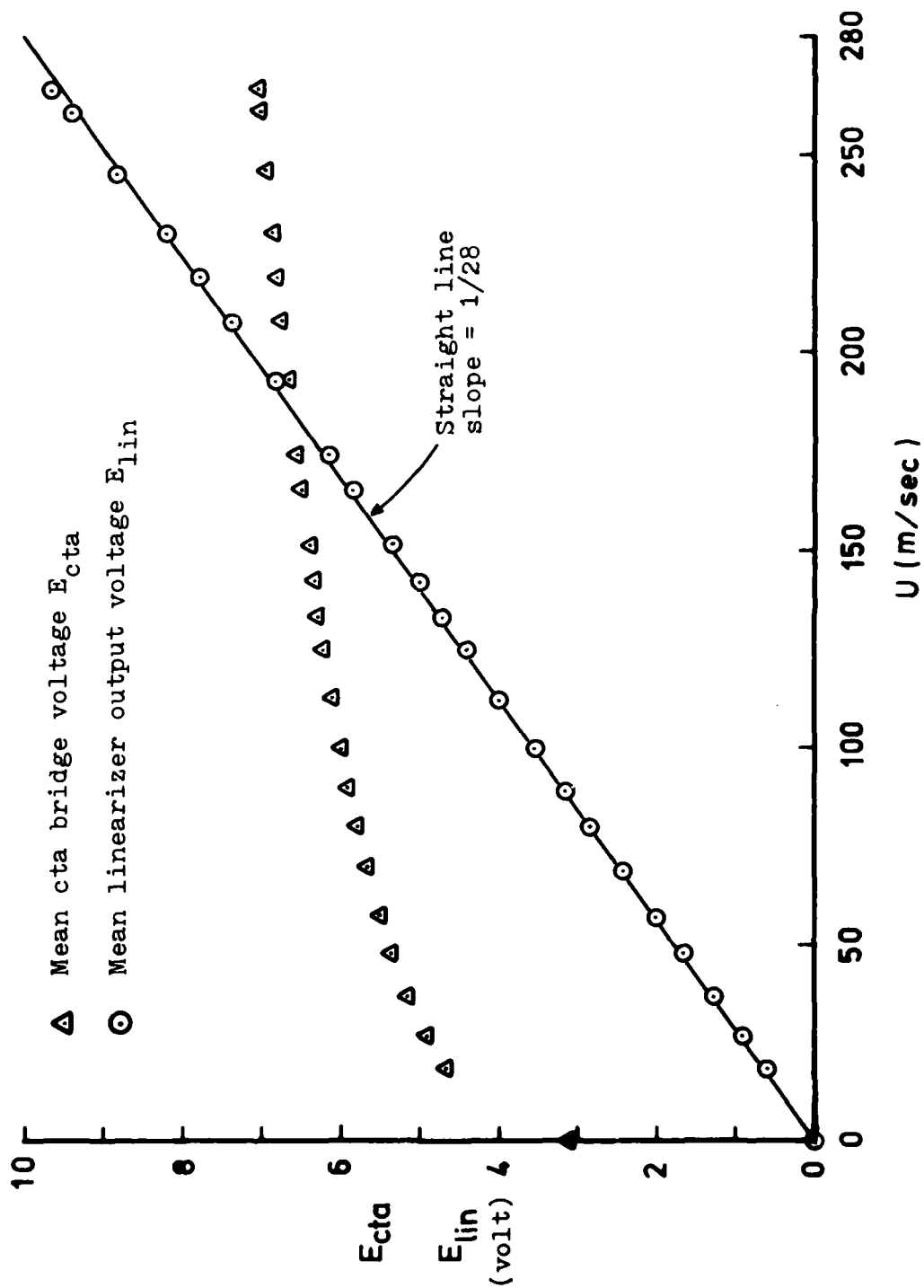


Figure 6 Calibration curves for the hot-wire

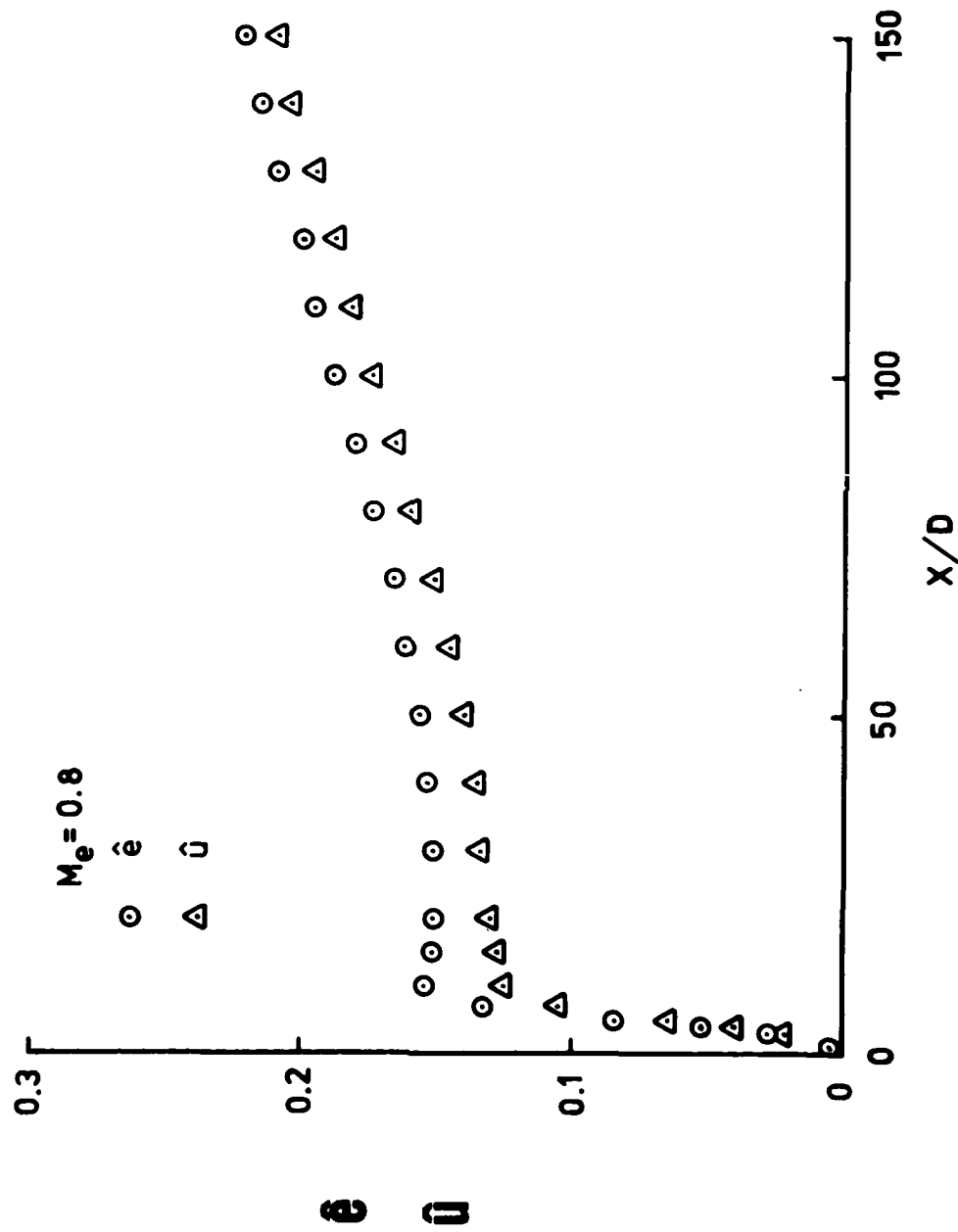


Figure 7 Measured r.m.s. intensity \hat{e} and corrected turbulence intensity \hat{u} along the centerline of the rectangular jet at $M_e = 0.8$



(a)



(b)

Figure 8 The rectangular jet at exit Mach number of 0.8
(a) Hot-wire with its support in the flow
(b) No probe in the flow

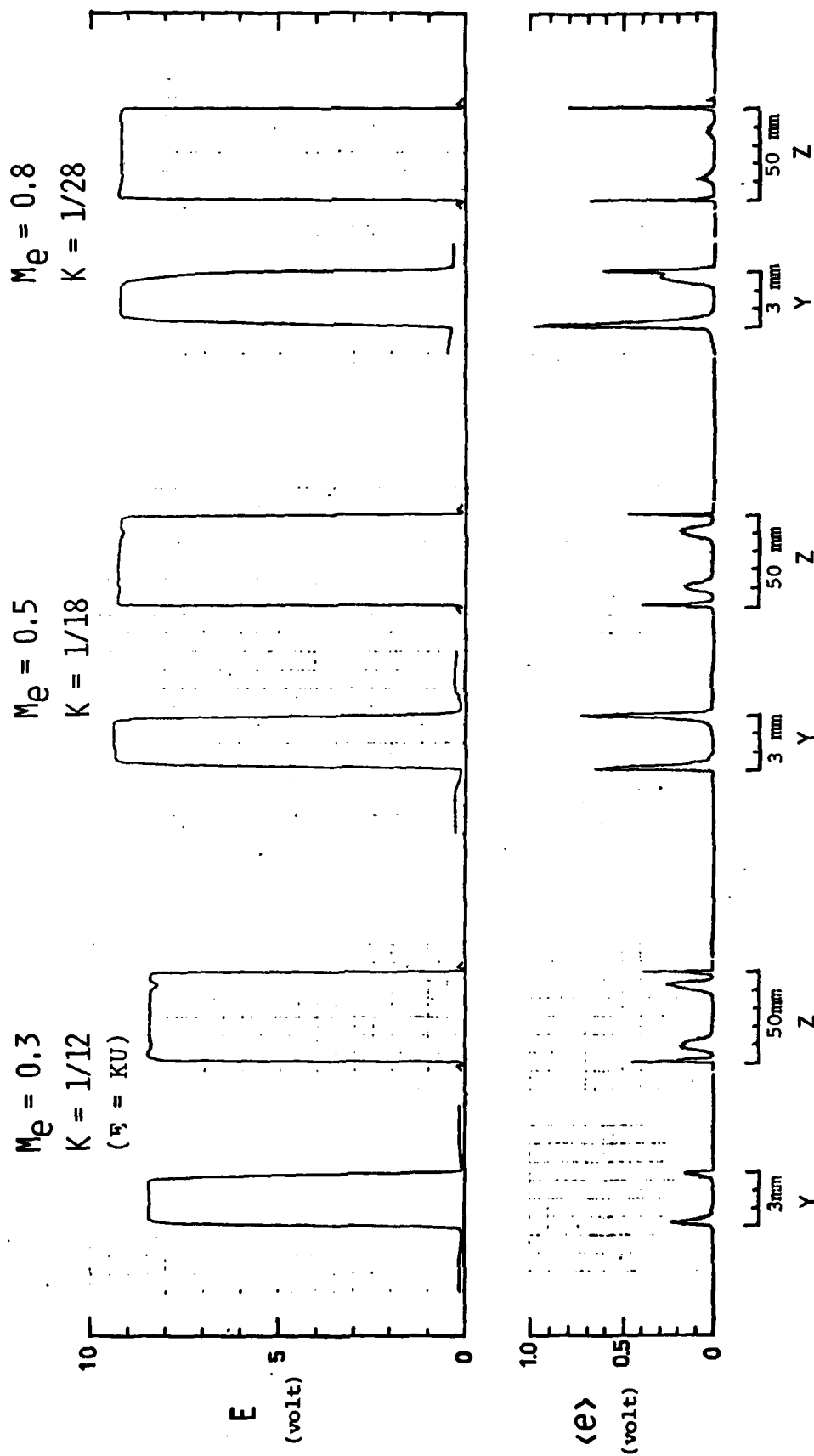


Figure 9 Mean and r.m.s. profiles of hot-wire voltage along Y and Z axes at the nozzle exit for $M_e = 0.3, 0.5$ and 0.8



(a) $M_e = 0.3$



(b) $M_e = 0.5$



(c) $M_e = 0.$

Figure 10 Schlieren photographs of the rectangular jet in the X,Y plane for different exit Mach numbers (M_e)



Figure 11 Schlieren photograph of the jet
in the X,Z plane for $M_e = 0.8$

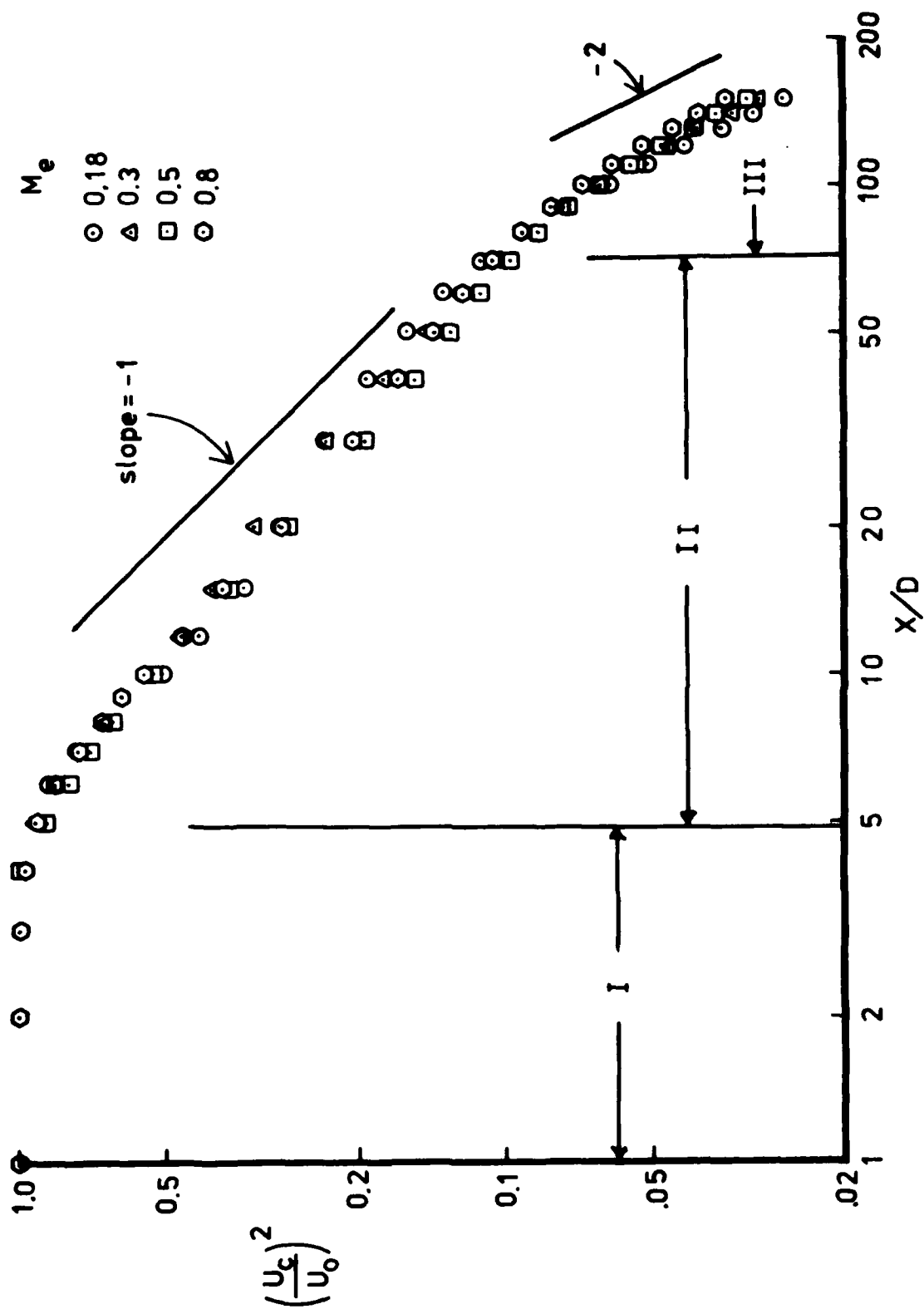


Figure 12 The decay of normalized centerline mean velocity of the jet for four exit Mach numbers

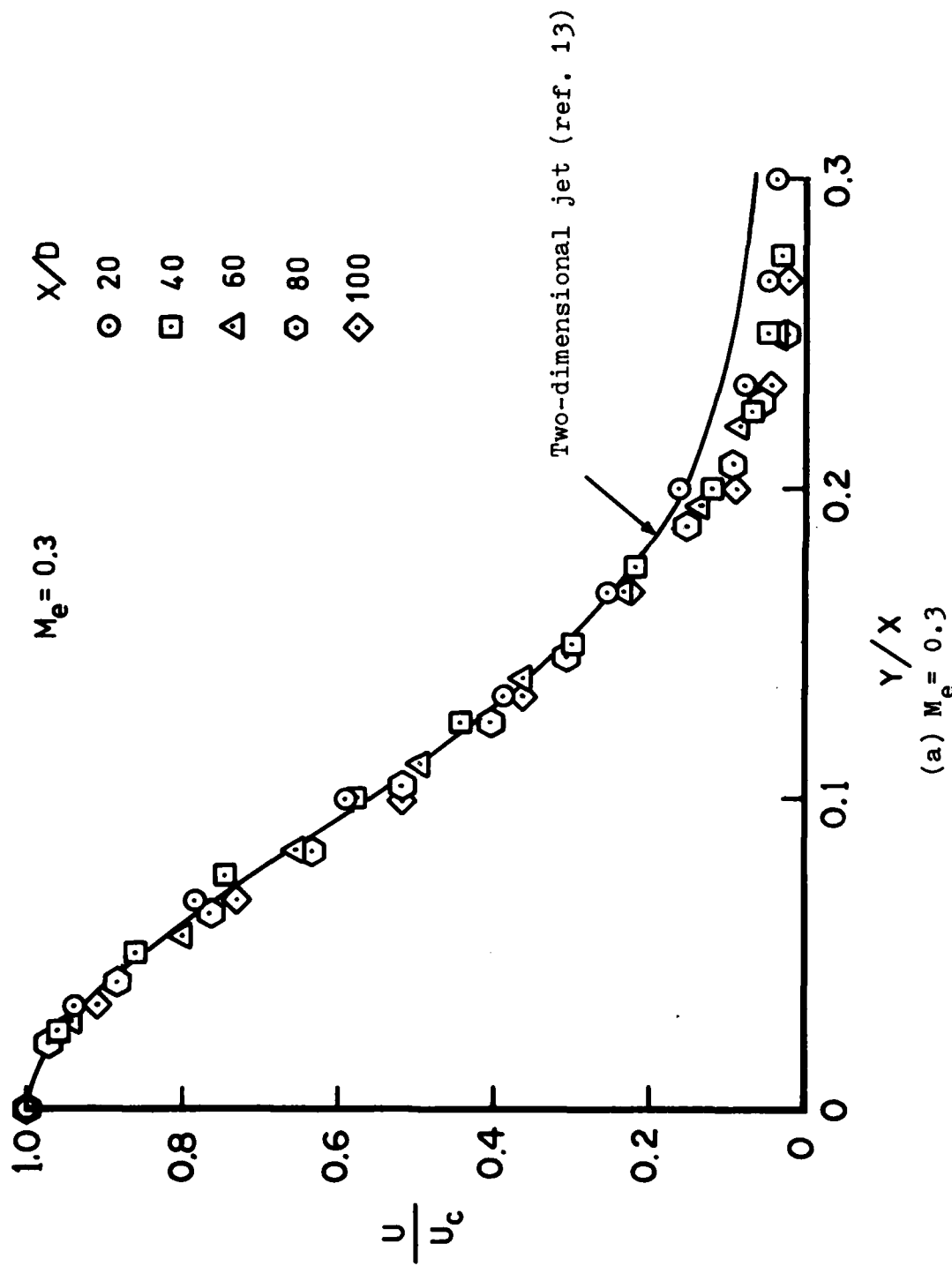
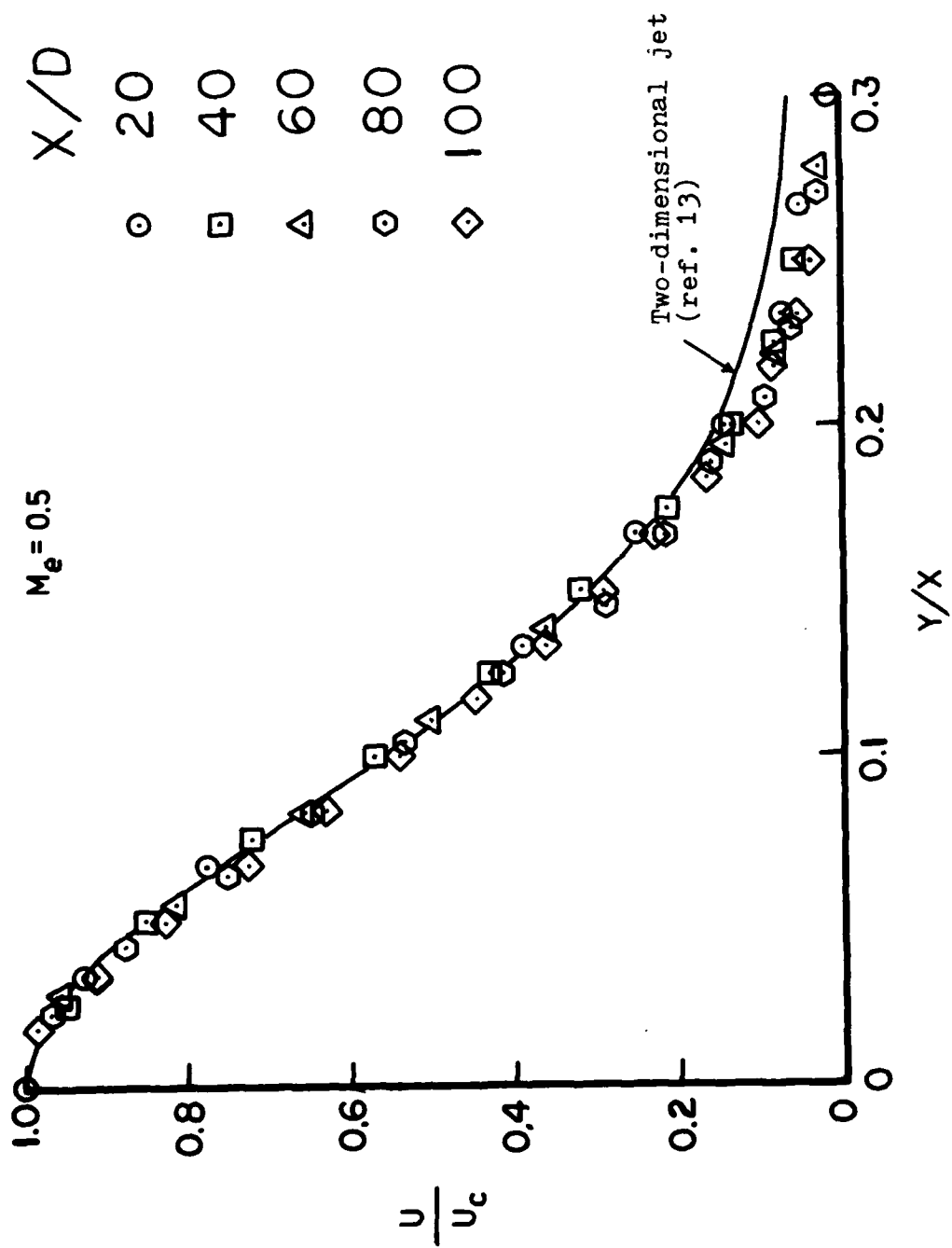
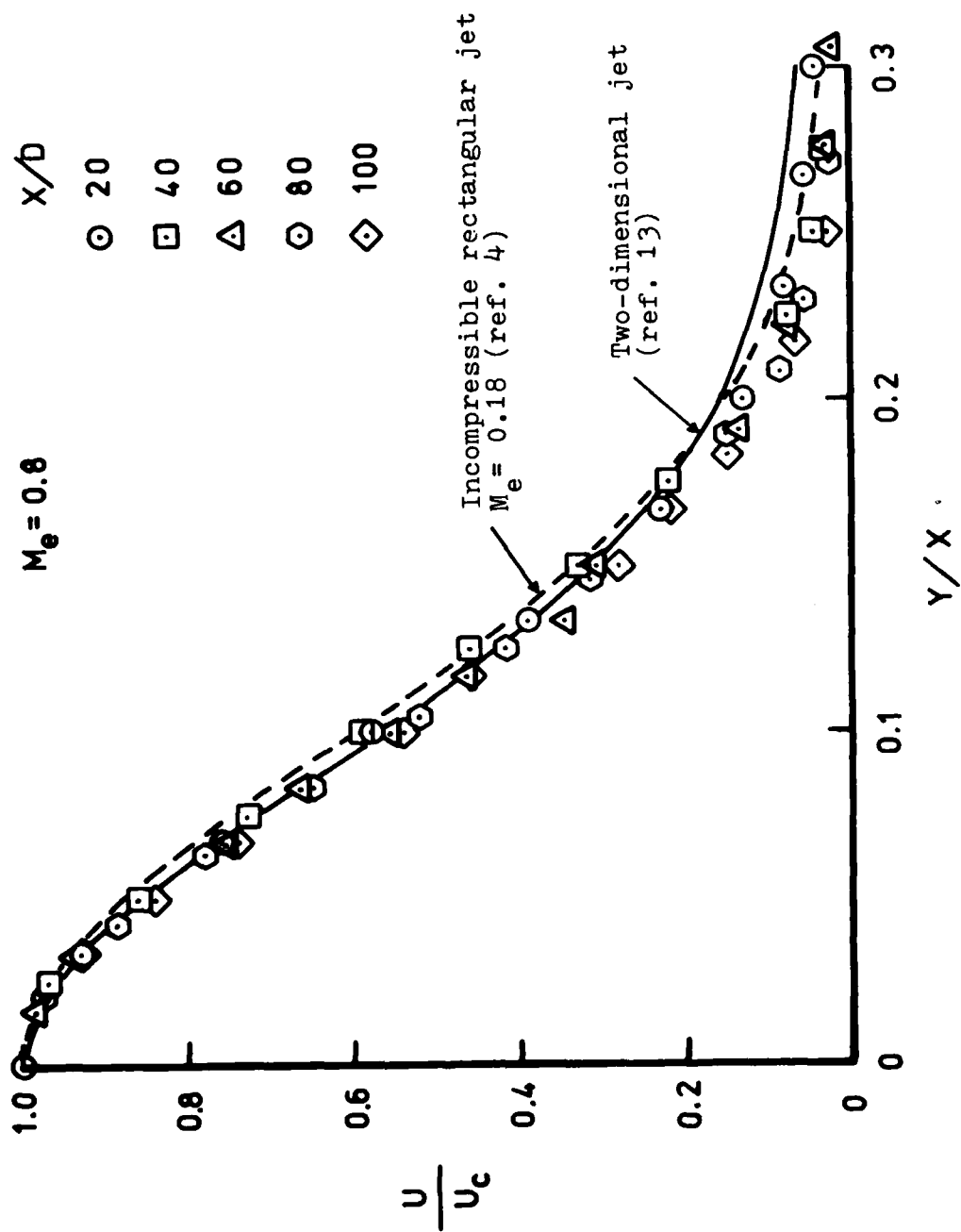


Figure 13 Mean velocity profiles in the central X,Y plane for three exit Mach numbers



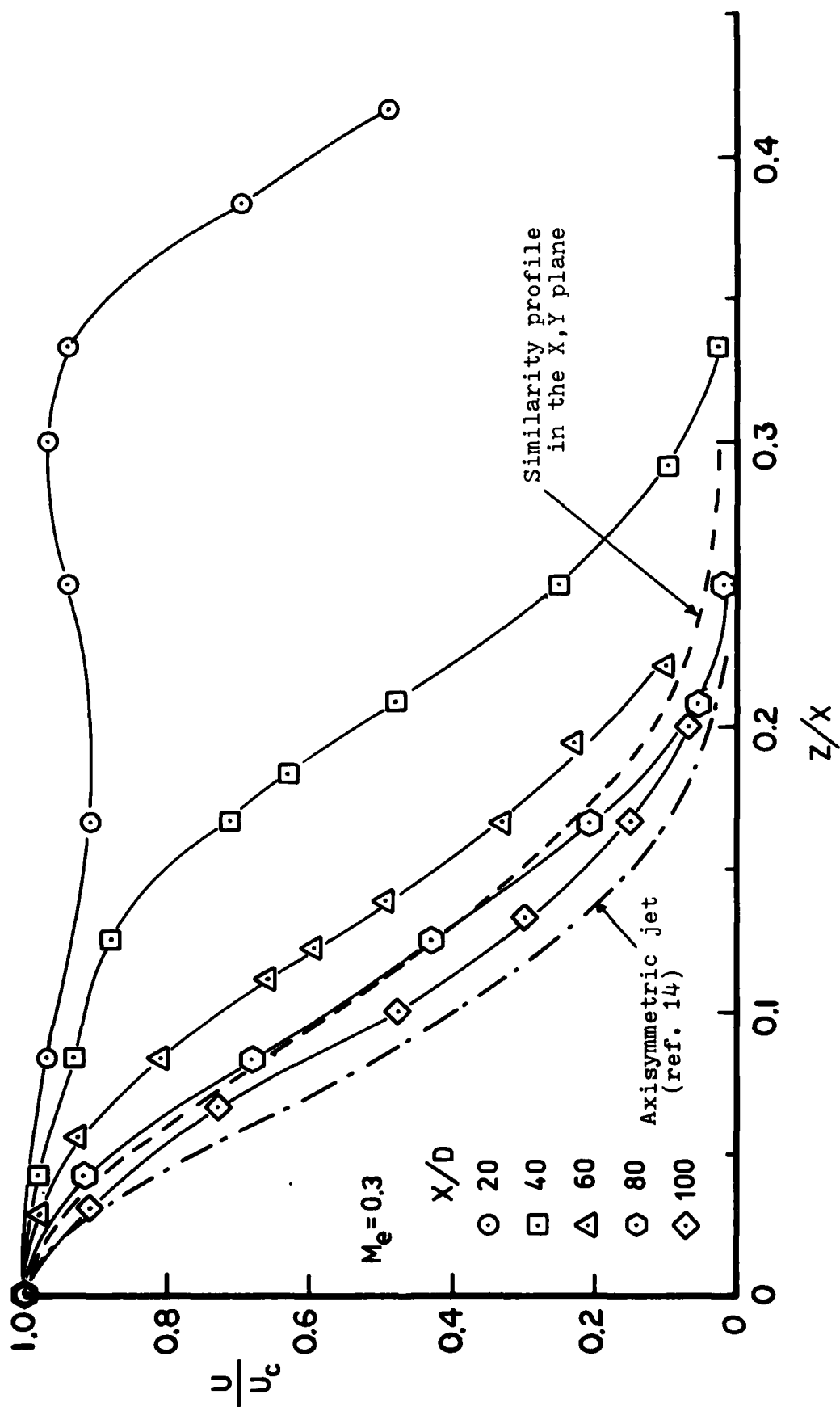
(b) $M_e = 0.5$

Figure 13 (continue)



(c) $M_e = 0.8$

Figure 13 (continue)



(a) $M_e = 0.3$

Figure 14 Mean velocity profiles in the central X, Z plane for three exit Mach numbers

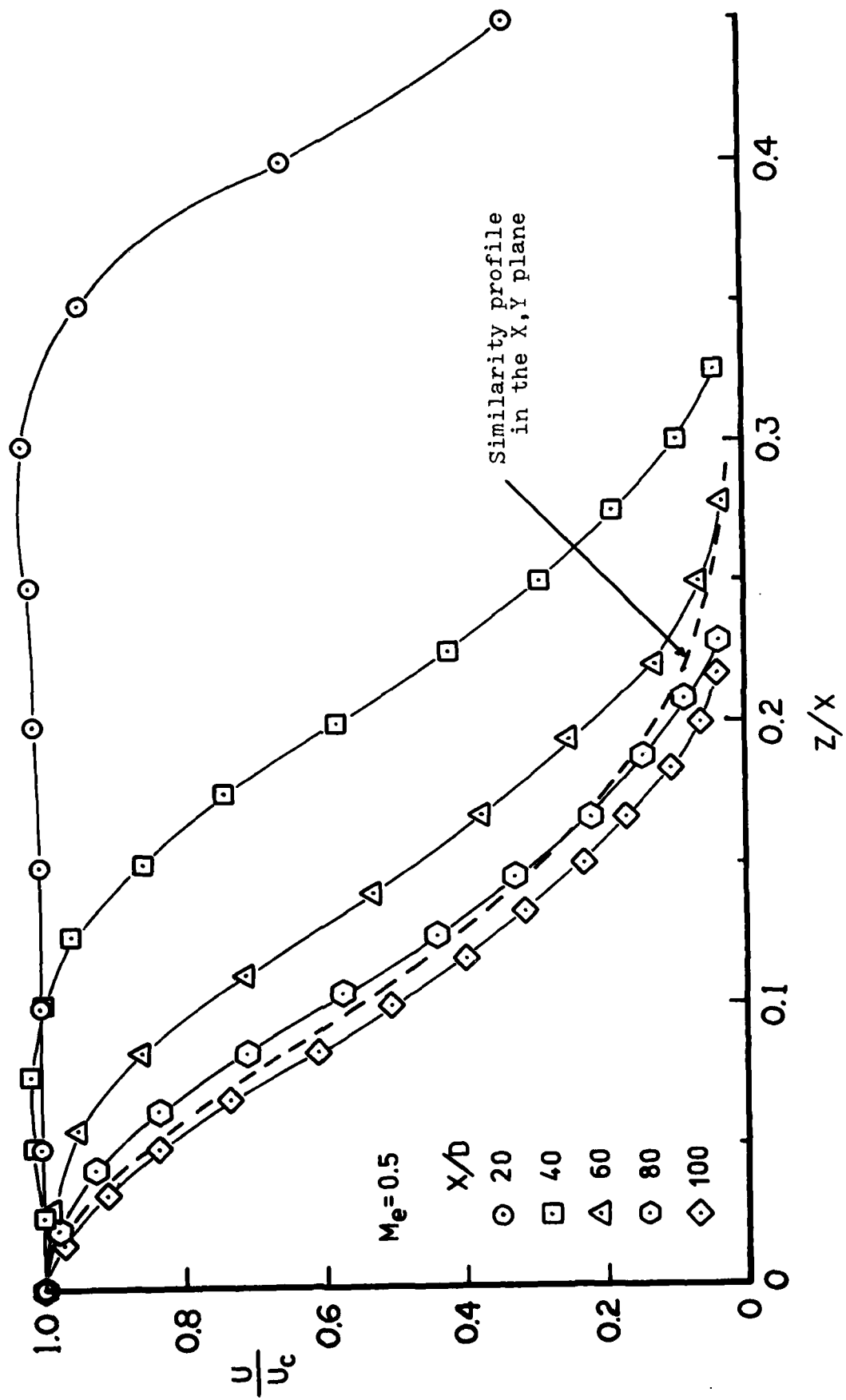


Figure 14 (continue) (b) $M_e = 0.5$

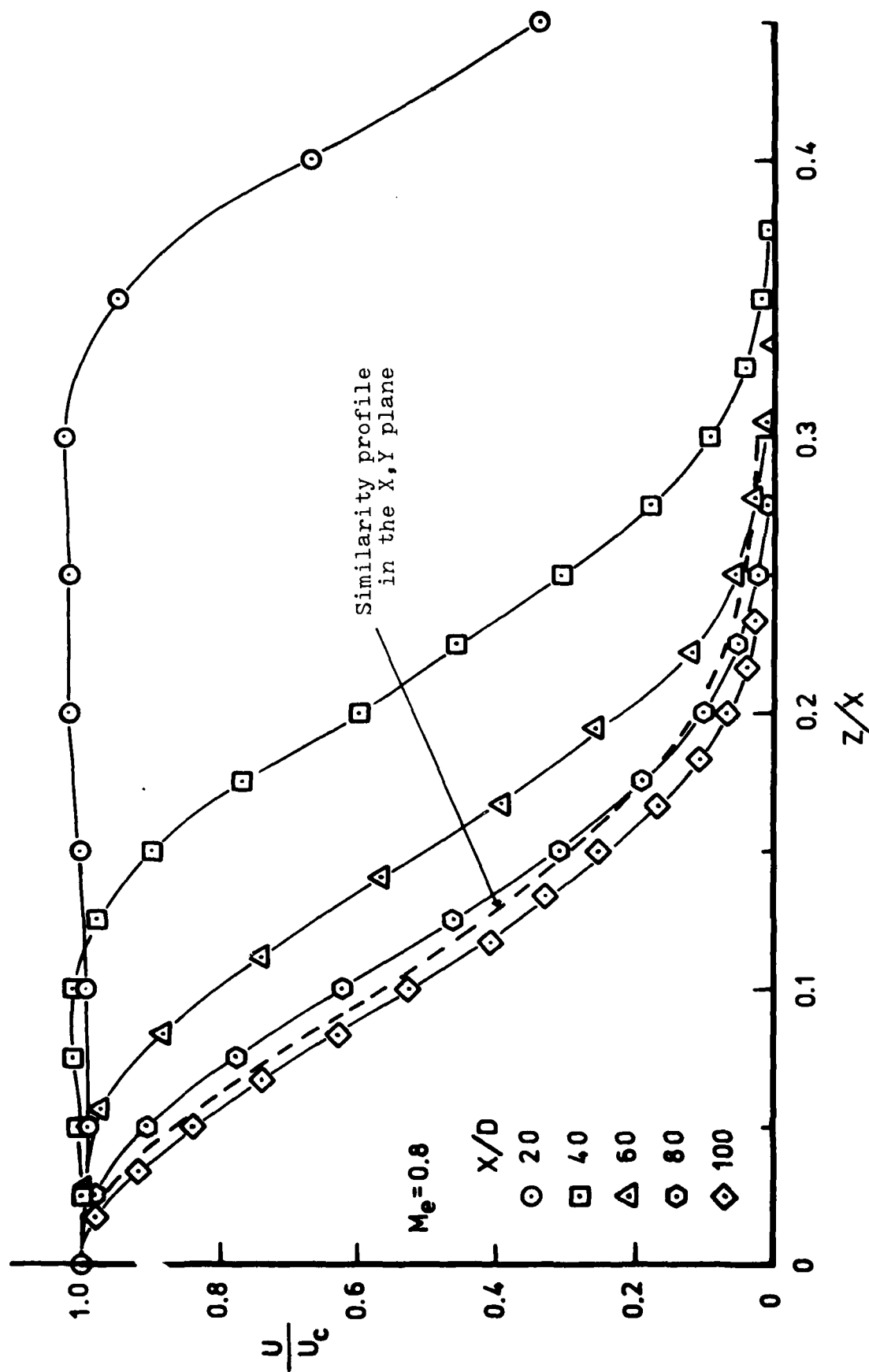


Figure 14 (continue) (c) $M_e = 0.8$

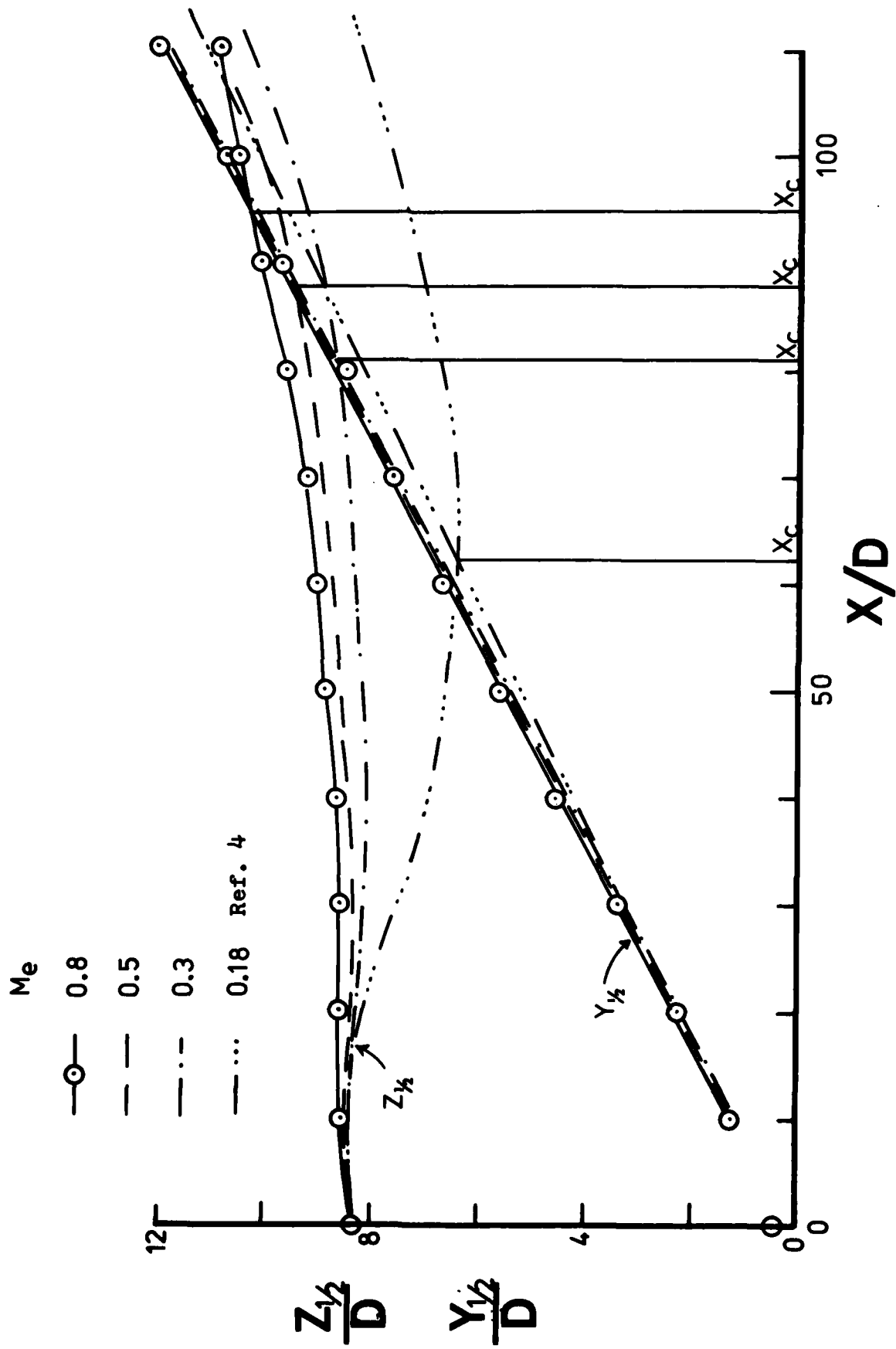


Figure 15 Growth of the jet with downstream distance for various exit Mach numbers

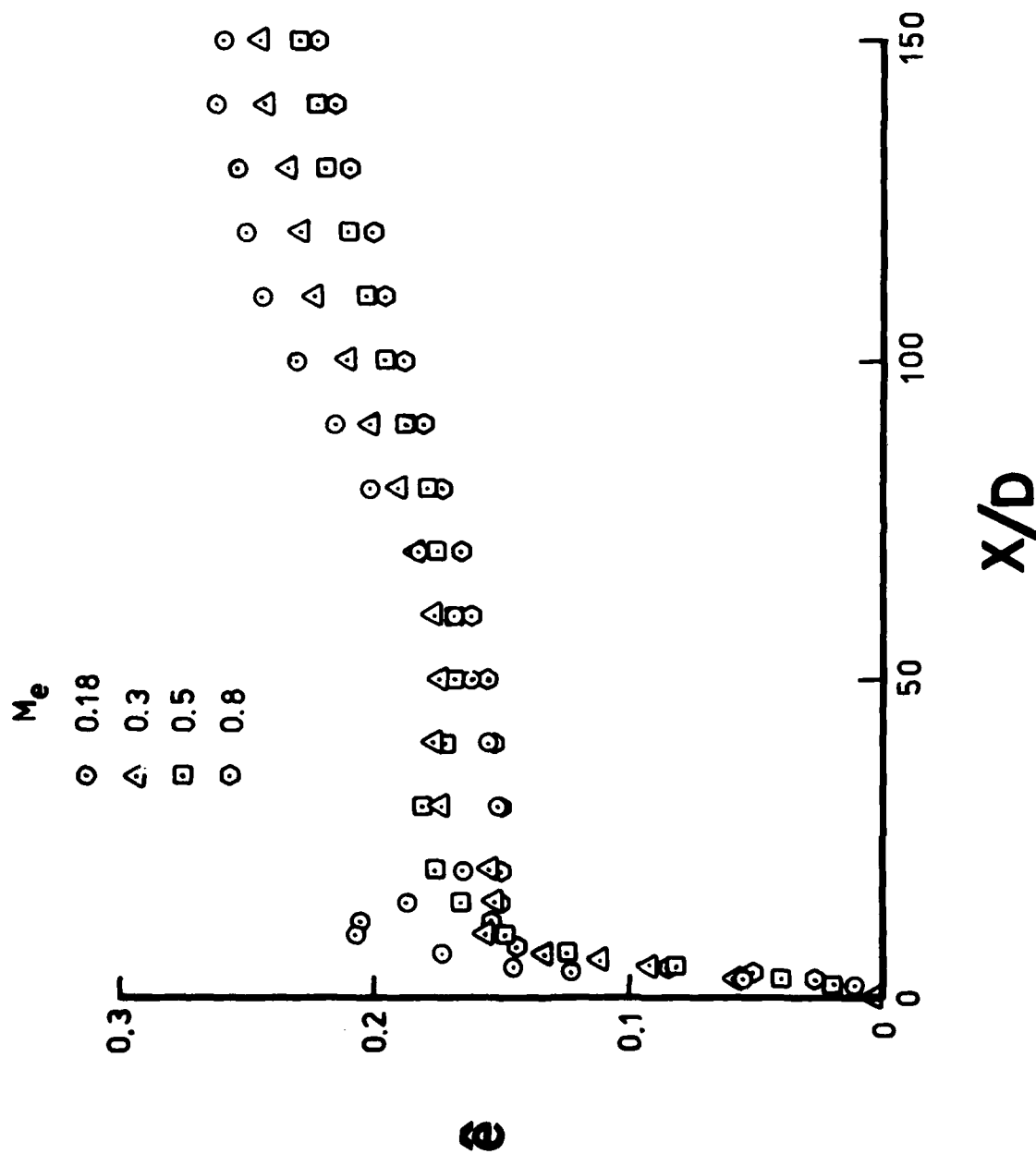


Figure 16 Variation of turbulence intensity along the centerline of the jet for different exit Mach numbers

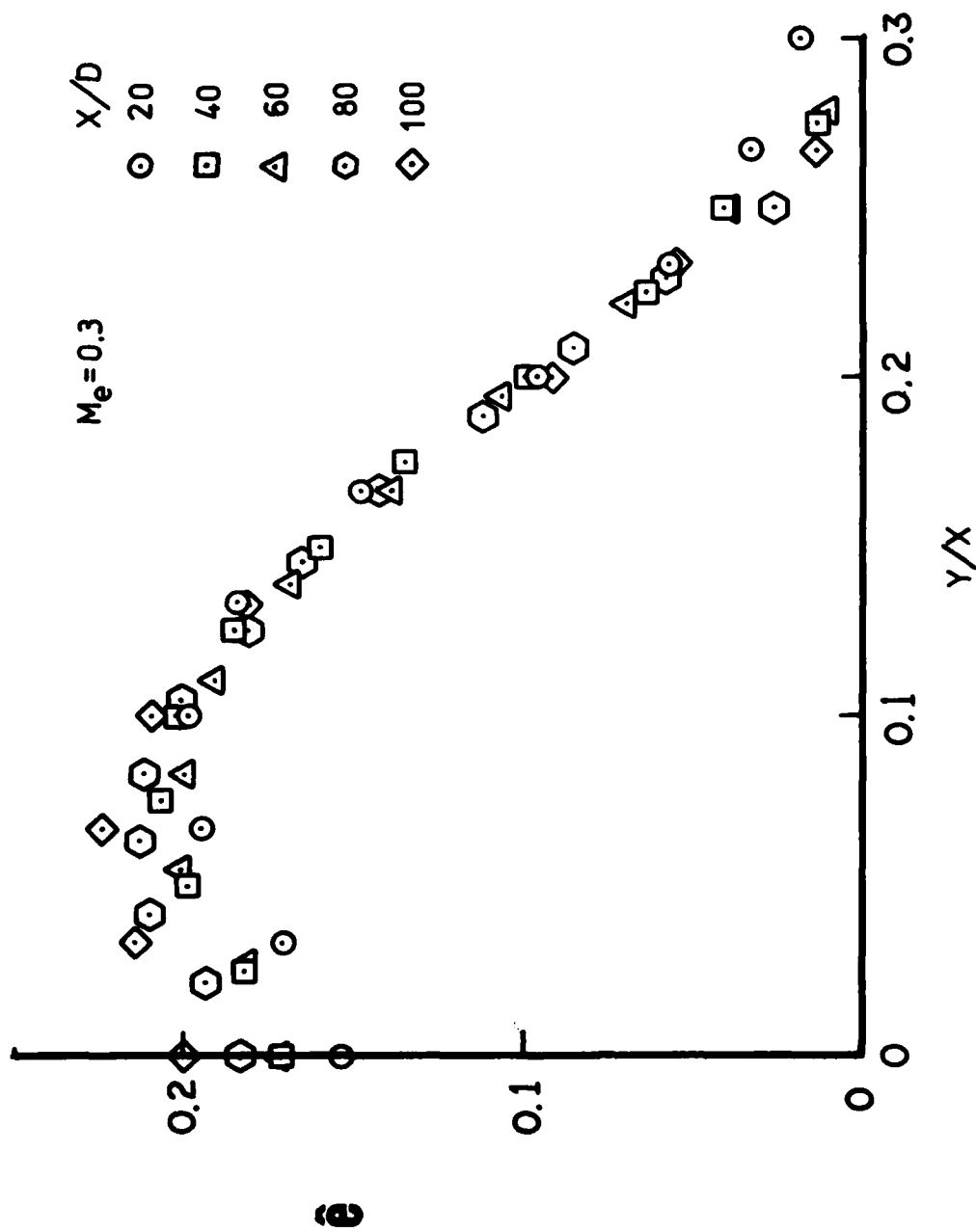


Figure 17 Distribution of hot-wire voltage fluctuation in the central X,Y plane for three exit Mach numbers

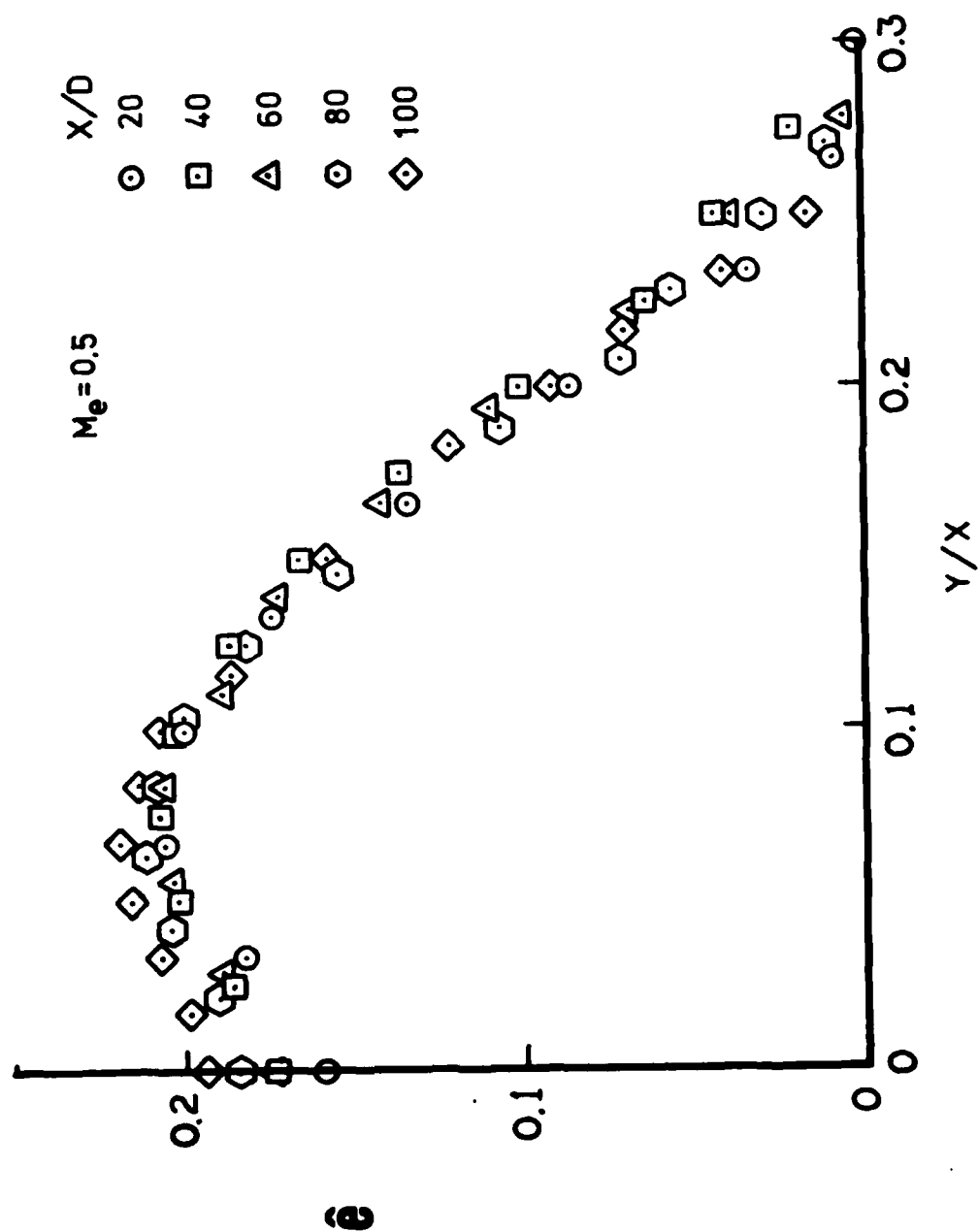


Figure 17 (continue) (b) $M_e = 0.5$

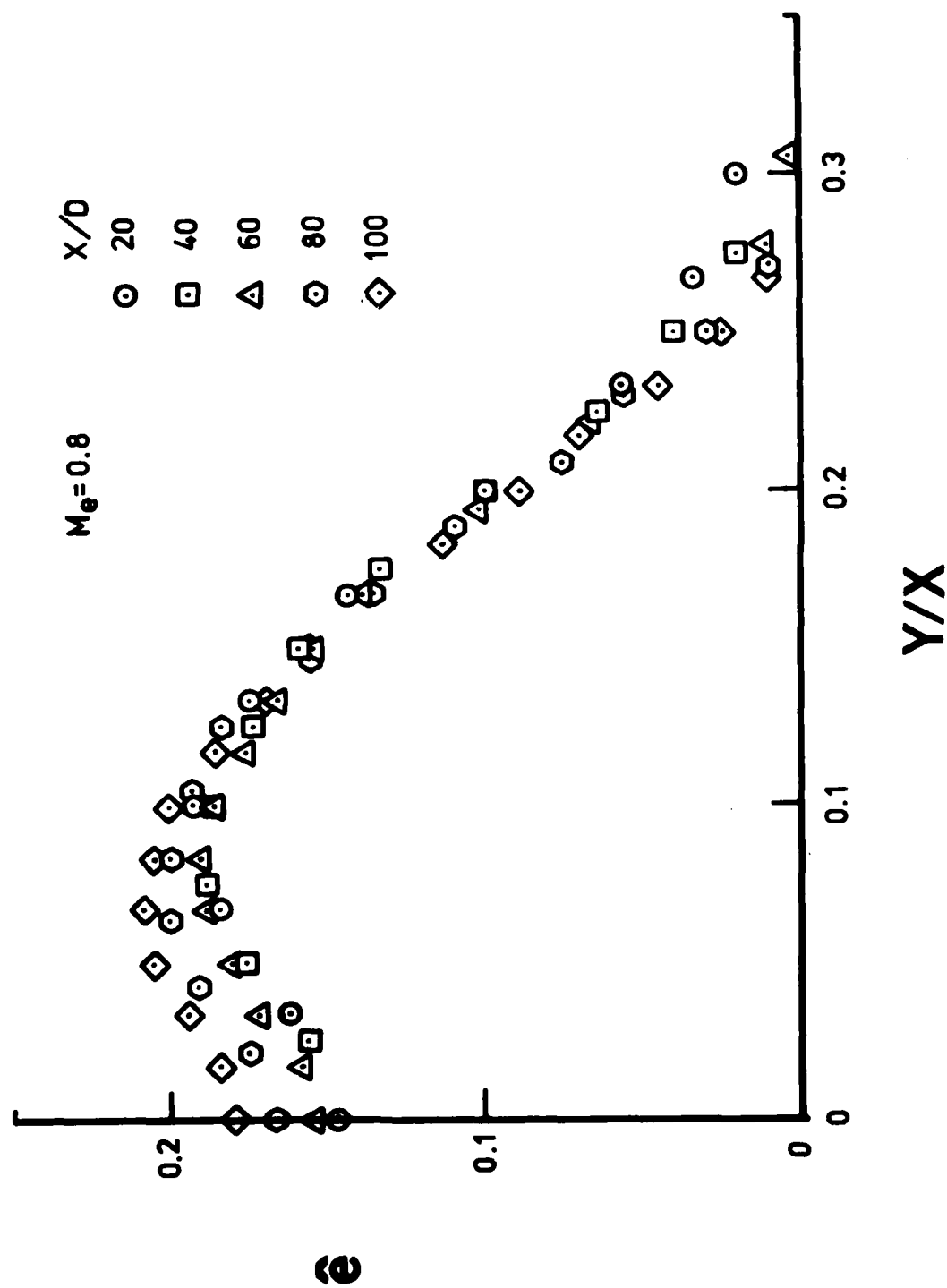


Figure 17 (continue) (c) $M_e = 0.8$

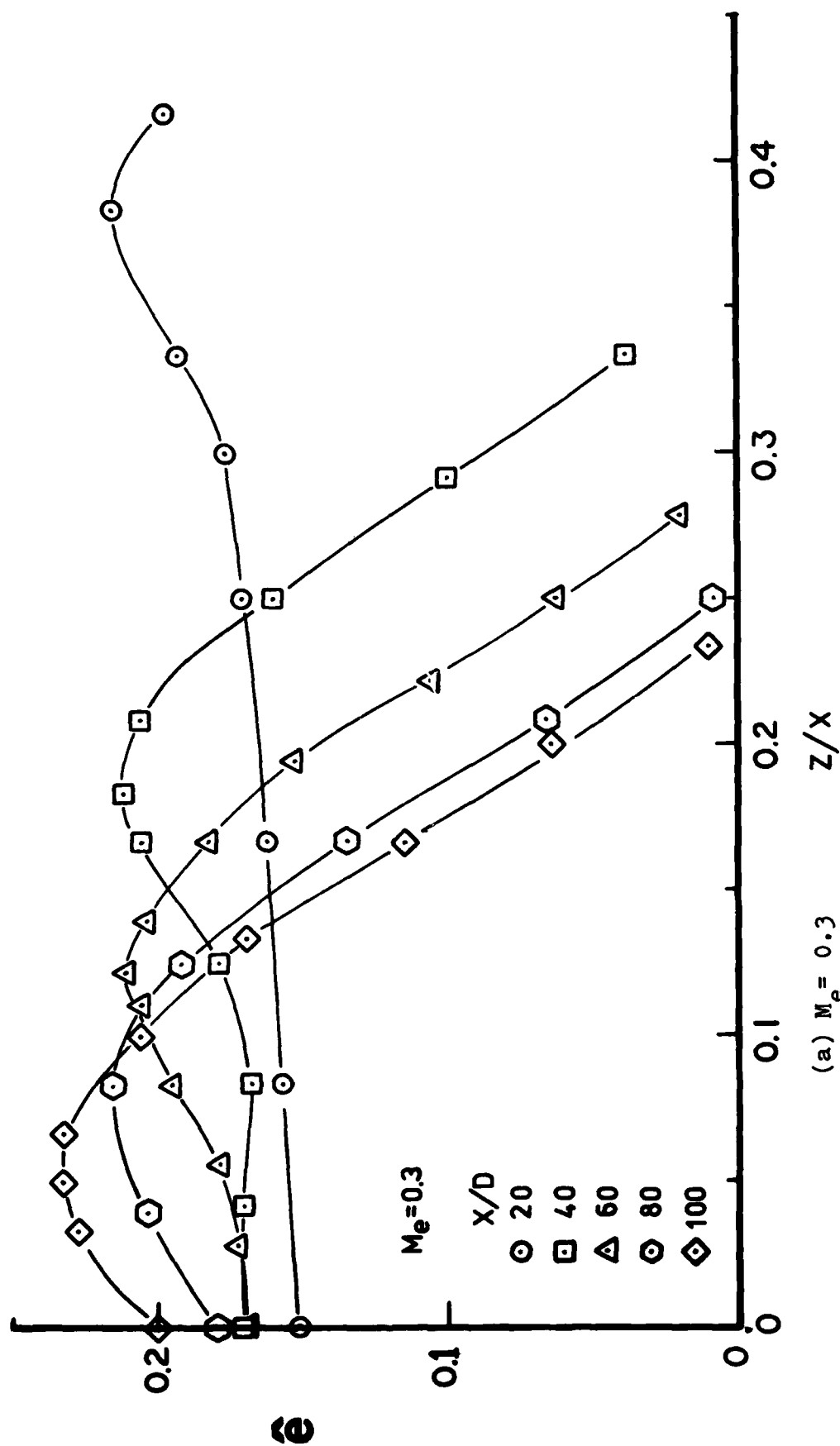


Figure 18 Distribution of hot-wire voltage fluctuations in the central X, Z plane for three exit Mach numbers

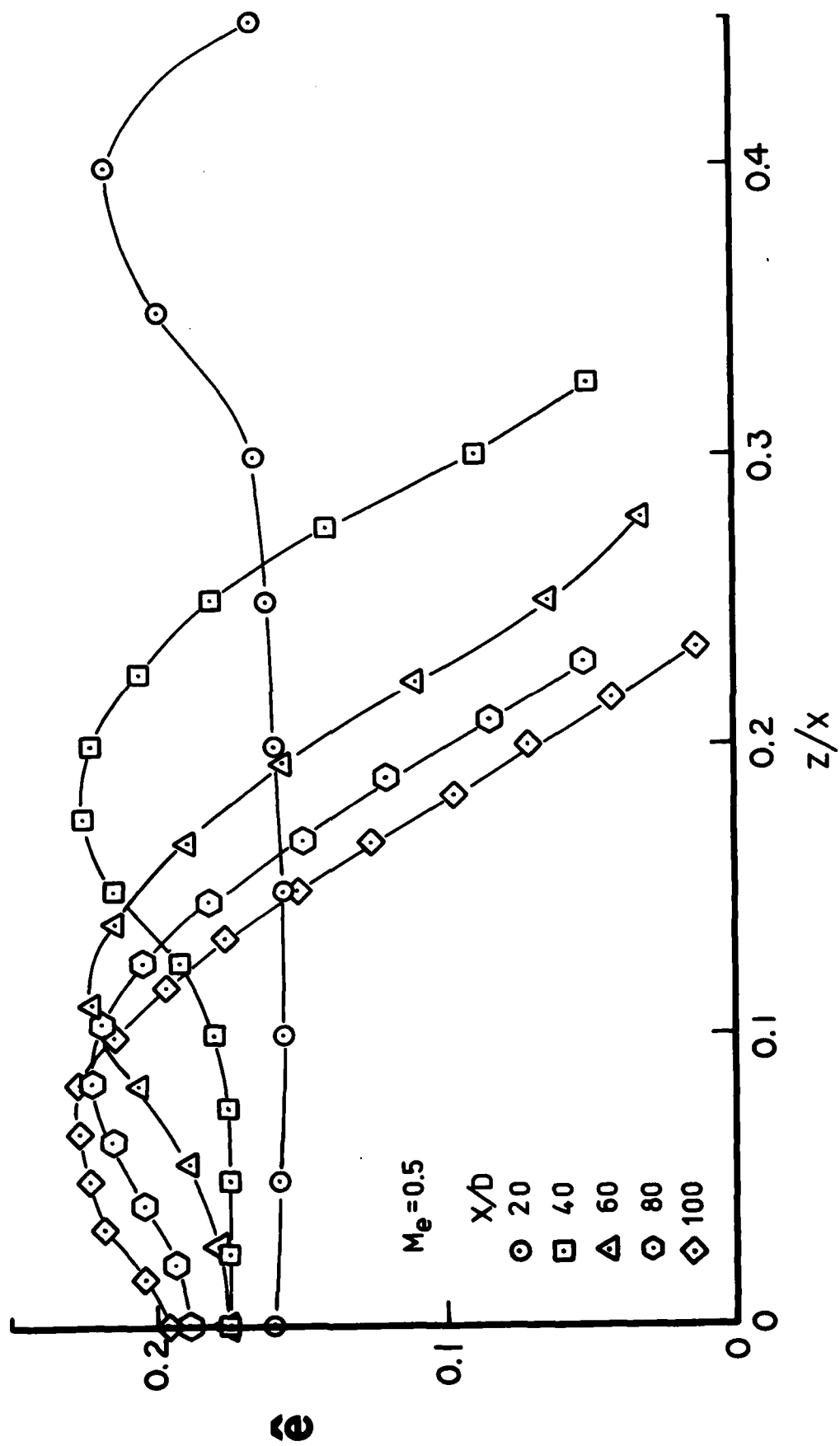


Figure 18 (continue) (b) $M_e = 0.5$

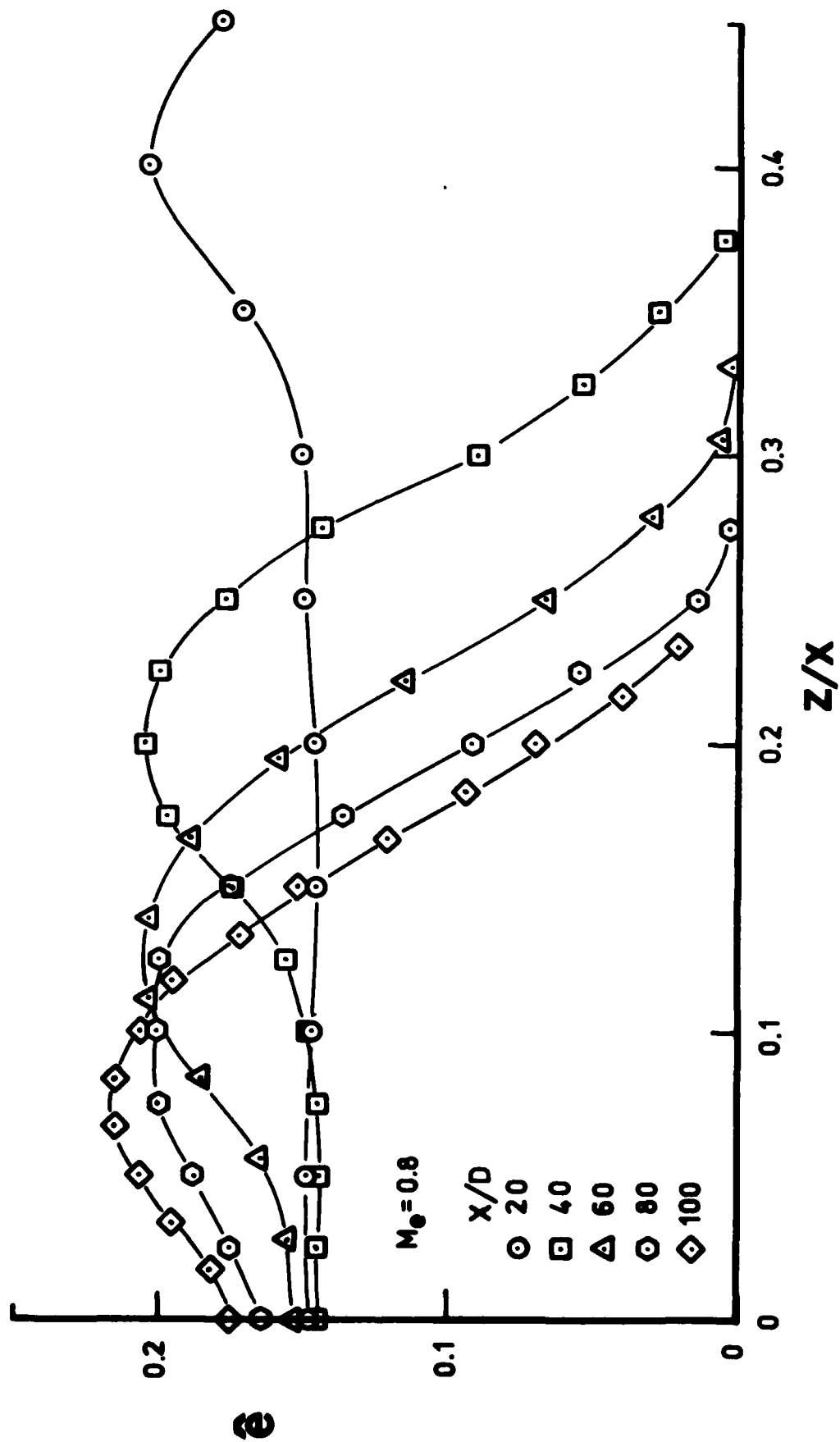


Figure 18 (continue) (c) $M_e = 0.8$

HOT-WIRE VOLTAGE

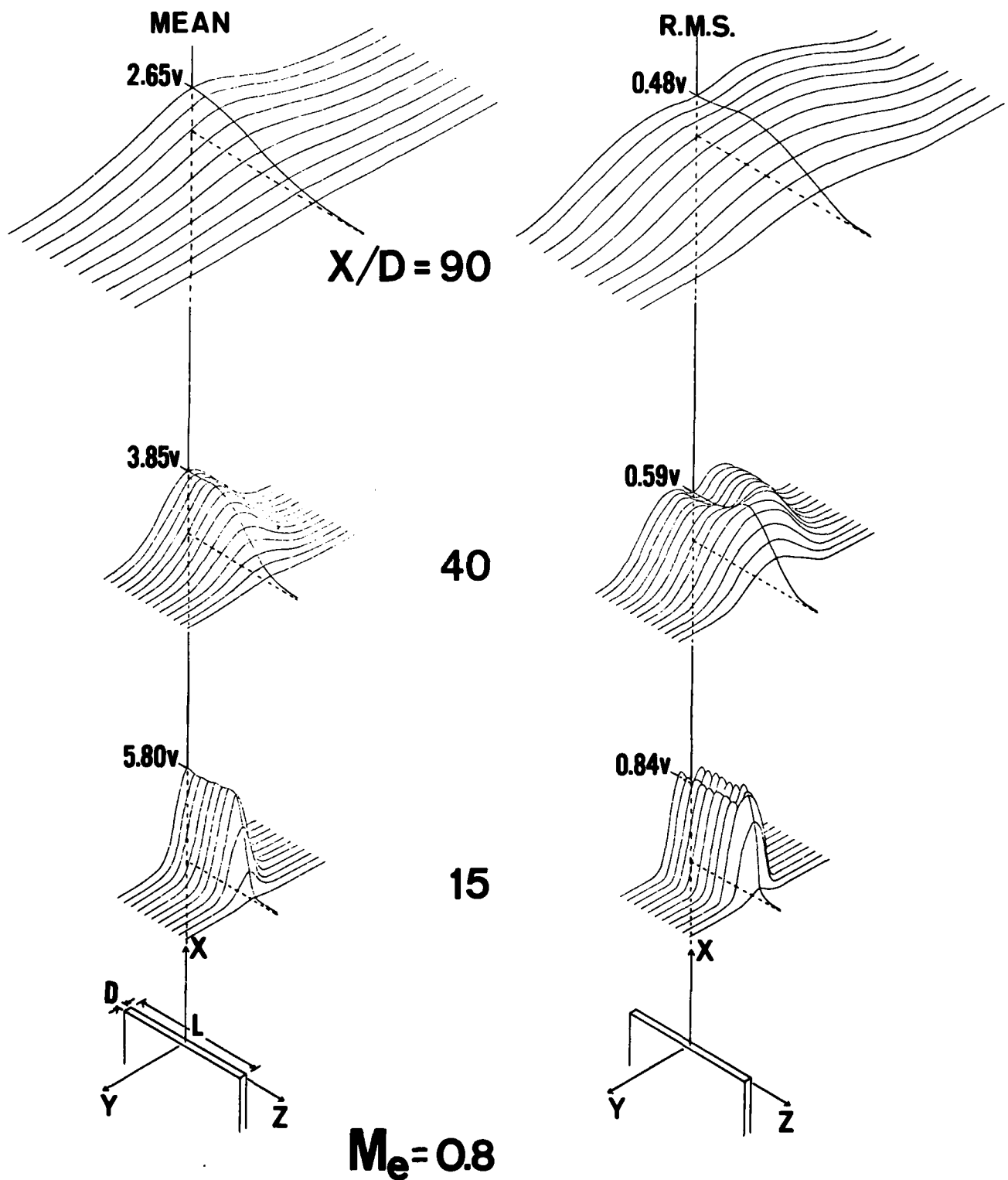


Figure 19 Isometric plots of the mean and r.m.s. hot-wire voltages for the jet at $M_e = 0.8$

DATE
ILME
—8